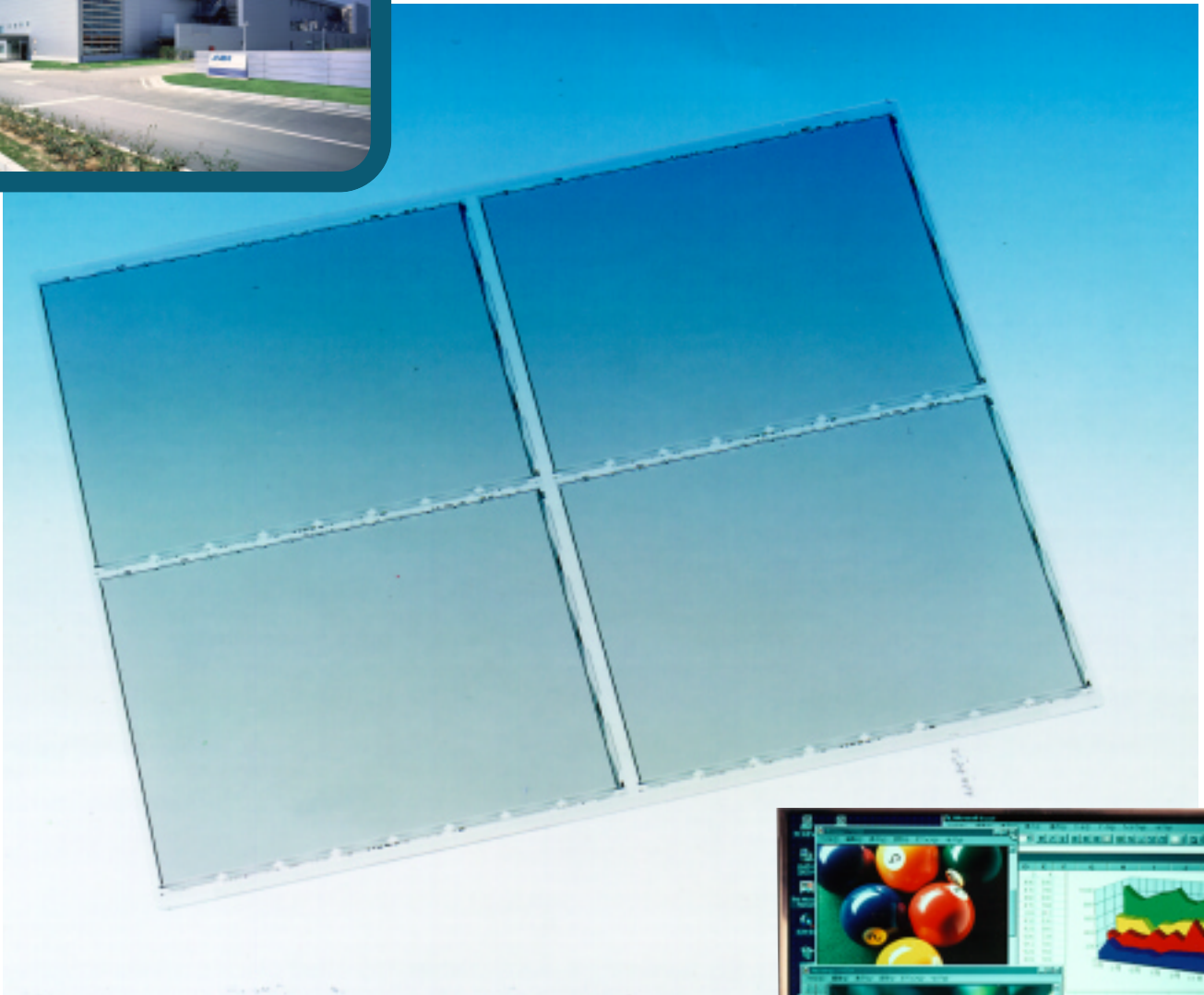


VOL. 83/JUN. 1998

mitsubishi electric

ADVANCE

Thin-Film Transistor LCDs Edition



Thin-Film Transistor LCDs Edition

CONTENTS

TECHNICAL REPORTS

OVERVIEW

Introducing the Special Edition on TFT-LCDs 1
by Makoto Morishita

The Concept and Vertical Ramp of the Shisui TFT-LCD Fabrication Line 2
by Ikuo Ogo and Kazuo Yoshida

Static Electricity Control and Glass-Cutting Technique for Narrow Margins 7
by Takayuki Ohishi and Dr. Kazushi Haruna

Design Technologies for Low-EMI Notebook Personal Computers 11
by Dr. Eishi Gofuku and Shinji Tanabe

An Optimum Pixel Light-Shield Pattern Design for TFT-LCDs 16
by Shigeru Yachi and Yasuo Fujita

An LCD with a Wide Viewing Angle for PC Monitor Applications 19
by Shin Tahata and Masaya Mizunuma

A 15.1-Inch XGA LCD Monitor 23
by Kazuyuki Iimura and Kunihiko Hashimoto

TECHNICAL HIGHLIGHTS

A TFT-LCD Panel for Thin Notebook Personal Computers 26
by Katsuhiko Honda and Mitsumasa Umesaki

NEW PRODUCTS 28

MITSUBISHI ELECTRIC OVERSEAS NETWORK

Color liquid-crystal displays (LCDs) must possess on/off switching characteristics adequate to ensure that the proper voltages are applied to the electrodes controlling pixel elements, and must use highly reliable thin-film transistors (TFTs). These are the basic requirements in forming TFT arrays.

The Shisui Factory (shown upper left) uses a single larger glass panel measuring 410 x 520mm (and only 0.7mm thick, shown in the center) to form four 12.1" TFT arrays. Each array comprises some 1.5 million elements. Color filter panels are laminated onto these arrays to form cells which are then filled with liquid-crystal material to complete display panels like that shown at the lower right.

Editor-in-Chief

Shin Suzuki

Editorial Advisors

Jozo Nagata
Toshimasa Uji
Kazumi Iwaizumi
Yasuo Kobayashi
Masao Hataya
Toshiharu Nozawa
Seiya Inoue
Hiroaki Kawachi
Akihiko Naito
Nobuo Yamamoto
Shingo Maeda
Toshikazu Saita
Akira Inokuma
Kouji Kadota

Vol. 83 Feature Articles Editor

Makoto Morishita

Editorial Inquiries

Kouji Kadota
Corporate Total Productivity Management
& Environmental Programs
Mitsubishi Electric Corporation
2-2-3 Marunouchi
Chiyoda-ku, Tokyo 100-0005, Japan
Fax 03-3218-2465

Product Inquiries

Kazumi Iwaizumi
Global Strategic Planning Dept.
Corporate Marketing Group
Mitsubishi Electric Corporation
2-2-3 Marunouchi
Chiyoda-ku, Tokyo 100-0005, Japan
Fax 03-3218-3455

Orders:

Four issues: ¥6,000
(postage and tax not included)
Ohm-sha Co., Ltd.
1 Kanda Nishiki-cho 3-chome
Chiyoda-ku, Tokyo 101-0054, Japan

Mitsubishi Electric Advance is published quarterly (in March, June, September, and December) by Mitsubishi Electric Corporation. Copyright © 1998 by Mitsubishi Electric Corporation; all rights reserved. Printed in Japan.

Overview

Introducing the Special Edition on TFT-LCDs



by Makoto Morishita*

Liquid-crystal display (LCD) devices, and in particular those driven by thin-film transistors (TFT-LCDs), are slim, lightweight, compact, and consume very little power. Recent strides in engineering have enabled the realization of larger screens, higher resolutions and wider viewing angles, and they are being adopted for use on the desktop as well as in portable applications. Mitsubishi Electric Corporation manufactures color TFT-LCDs and, jointly with Asahi Glass Company, has founded Advanced Display Inc. (ADI) which develops and markets large-screen direct-view products with screen sizes of 10" and above. In addition to development activities by ADI itself, research staff at Mitsubishi Electric and the corporation's Manufacturing Engineering Center, with those of Asahi Glass, provide in-depth support for the development of a wide range of technologies essential to TFT-LCD production, from panel manufacture to module assembly.

ADI's state-of-the-art Shisui Factory is provided with automated lines for integrated production from panel manufacture through module assembly. It commenced mass production just three months after delivery of the production equipment. ADI's technology is being provided to Taiwan's Chunghwa Picture Tube Company as part of a global business strategy.

Mitsubishi Electric views LCD modules as a tool for use in man-machine interfaces. Recognizing that these modules are entire systems comprising semiconductors, panels, circuits and backlights, we are conducting development in four major areas critical to such systems—performance, quality and price, system functions, and friendliness to the environment. Together with efforts to extend the performance limitations of displays, the Shisui Factory is using production lines that can flexibly adapt to changes in products and processes in order to achieve higher productivity and reduce costs, utilizing optimized factory automation as a key plant design concept to ensure stable product quality. LCDs are a byword for the efficient use of resources and environmental friendliness thanks to their low power consumption, but the plant is also grappling with the problems of electromagnetic interference (EMI), which have drawn attention in this age of digital devices, as well as issues of power consumption, recycling, and waste-liquid processing in plant operations.

Mitsubishi Electric is also drawing on its mainstream semiconductor technologies for the development of LCDs which operate as information display devices that combine video and text to meet the demands of the multimedia age. □

*Makoto Morishita is with the LCD Marketing Division.

The Concept and Vertical Ramp of the Shisui TFT-LCD Fabrication Line

by Ikuo Ogo and Kazuo Yoshida*

While the newest active-matrix liquid-crystal display (LCD) products boast features such as wide viewing angles and higher aperture ratios, to successfully market these products requires that production costs face the same scrutiny as established LCD products. A manufacturing line for advanced 12.1" LCDs, which are projected to be the most popular size for notebook computer applications at least through 1998, was constructed at the Shisui Factory of Advanced Display Inc. The fully automated line was designed for a three-month vertical ramp from equipment delivery to mass production. To satisfy these requirements, Mitsubishi Electric needed to develop technologies for fabricating four 12.1" displays on a 410 × 520mm sheet with a 3.25mm border. This report describes the design concepts and process technologies used at the Shisui Factory.

Design Goals

Facility construction for the line began in spring of 1995 and production began a year later in spring of 1996. The sheet size was boosted from the standard 400 × 500mm size of the 2.5 phase line to a unique 410 × 520mm, which supports the production of four 12.1" panels. Goals for the line were as follows:

HIGH PRODUCTIVITY, LOW COST. Considering the large potential demand for LCD panels in PC monitor applications, we targeted efficient production of 12.1" panels, which are expected to have substantial market longevity, while attempting to reduce facility costs by keeping the glass sheet dimensions as small as possible.

FLEXIBLE, AUTOMATED PRODUCTION. Automated manufacturing and information systems similar to those used in semiconductor production were implemented in a flexible system designed to adapt to future process changes, extending the production line's useful life.

VERTICAL RAMP UP. To facilitate recovery of investment cost, the line was designed to enter operation three months after the production equipment was delivered and to achieve full-

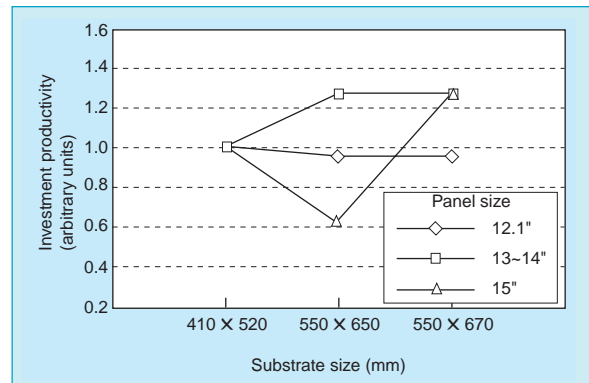


Fig. 1 Productivity of investment for three substrate sizes.

capacity production six months after startup.

Glass Panel Size

Panel sizes of 400 × 500mm, 450 × 550mm and 550 × 650mm were considered. The final 410 × 520mm size was selected based on the following criteria: LCDs with screen sizes of 11.3~12.1" were seen as mainstream products. Based on minimum sheet size, four-per-sheet 12.1" screens and two-per-sheet 15.1" screens appeared to offer the best return on investment, with the ideal sheet size being 450 × 550mm. However, transport equipment for this sheet size was anticipated to cost as much as that for large 550 × 650mm sheets. Furthermore, equipment for handling 550 × 650mm panels was not fully developed, and would have required longer setup times. In contrast, proven equipment for 400 × 500mm panels was already available and could be readily modified to handle 410 × 520mm sheets. The projected investment productivity for 12.1~15.1" panels based on this sheet size far surpassed that for 550 × 650mm sheet technology (Fig. 1).

The investment productivity (TE) can be calculated as:

$$TE = EEC \times ETP \times ENP \times EBC,$$

where EEC = equipment cost for 410 × 520mm sheets divided by equipment cost for other-sized sheets, ETP = throughput for other-sized sheets

*Ikuo Ogo is with Advanced Display Inc. and Kazuo Yoshida the Manufacturing Engineering Center.

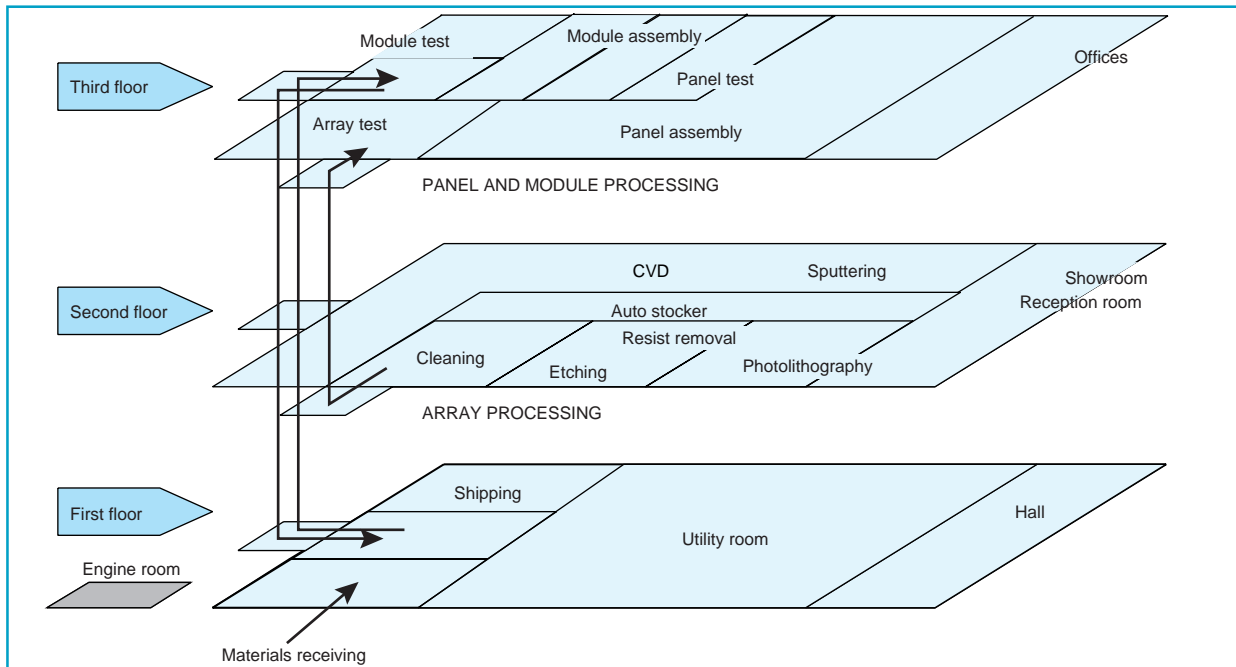


Fig. 2 Line layout.

divided by throughput for $410 \times 520\text{mm}$ sheets, $\text{ENP} = \frac{\text{number of panels for other-sized sheets}}{\text{number of panels for } 410 \times 520\text{mm sheets}}$, and $\text{EBC} = 1 - 0.25 \times [1 - \frac{\text{footprint } (410 \times 520\text{mm})}{\text{footprint of other-sized sheets}}]$.

The factory construction cost was assumed to be 25% of the total investment, standardized to the projected investment for a $410 \times 520\text{mm}$ sheet size. Fabrication of four 12.1" panels on a $410 \times 520\text{mm}$ sheet requires the use of a narrower insulating border at the sheet edges. This requires uniform coating, photolithography and etch characteristics right up to the sheet's 3~4mm border, along with better defect control and prevention of yield losses associated with the "scribe and break" process. Faced with the choice between working to improve process uniformity at sheet borders or investing the time to solve problems in $550 \times 650\text{mm}$ equipment, we elected to adopt a $410 \times 520\text{mm}$ sheet size.

Line Configuration

The Shisui Factory represents the industry's first

fully automated TFT-LCD production line. While semiconductor processing plants have employed fully automated transport for some years, TFT-LCD plants have lagged due to problems such as lower return on investment and added setup complexities that delay startup. However, manual handling procedures are complicated, and we judged that full automation would lead to higher quality.

Fig. 2 shows the configuration of the Shisui Factory. The second floor has clean rooms for fabricating the TFT array, and the first floor provides space for returning the processed sheets. Fig. 3 illustrates the plant's automation system.

Early Startup

Several unpredictable elements affected the vertical ramp of Shisui's 12.1" four-panel processing line, including new specification equipment and a new automation system. Delays were minimized by resolving most of the problems prior to delivery during equipment design and production phases. Fig. 4 compares pre-installation and post-installation problems. This

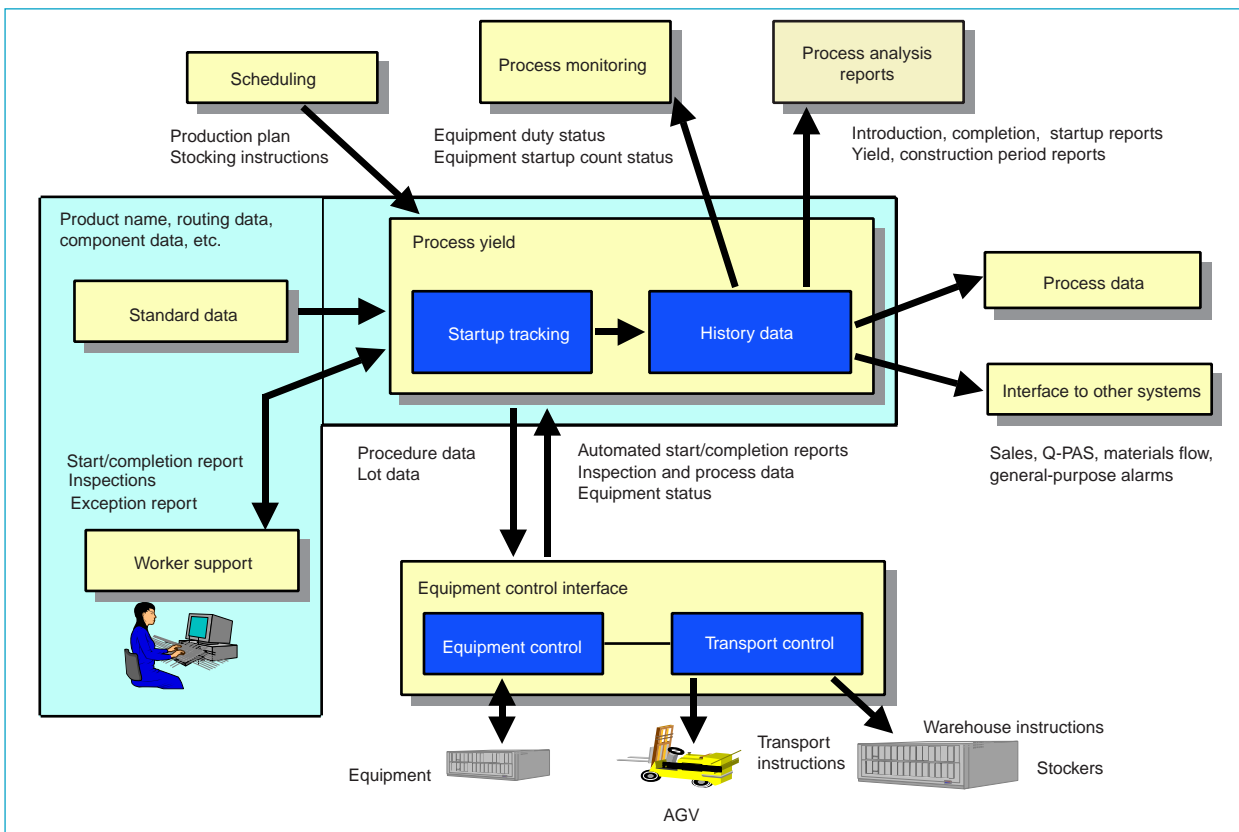


Fig. 3 Automation system concept.

approach enabled us to achieve the line startup target. Fig. 5 shows the yield of the TFT array fabrication line in the months following line startup.

Improving Process Uniformity at Panel Borders

Implementation of the plant design concept depended on high-yield processing of a 410 × 520mm sheet containing four 12.1" LCD panels, uniform processing up to the 3~4mm border and the suppression of static electricity. Studies led to the layout shown in Fig. 6.

FILM PRODUCTION. Chemical vapor deposition (CVD) and sputtering processes are used to fabricate the TFT arrays. An isothermal CVD unit permits flawless films to be deposited reliably right up to the substrate edges. The glass is held horizontally and mask materials for holding the

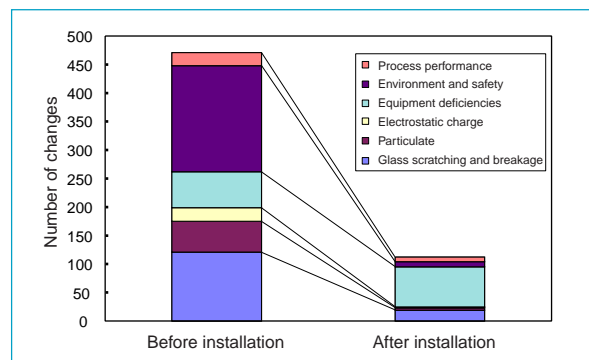


Fig. 4 Equipment changes before and after installation.

glass to the lower electrode are not needed, in contrast to cold-chamber units where a mechanism for holding the glass firmly to the lower electrode is required to achieve uniform temperature. The CVD unit also has a self-clean-

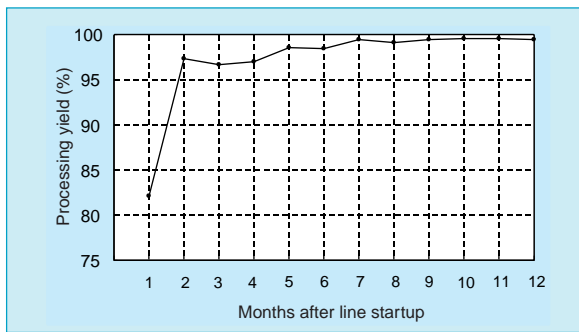


Fig. 5 Sheet processing yield.

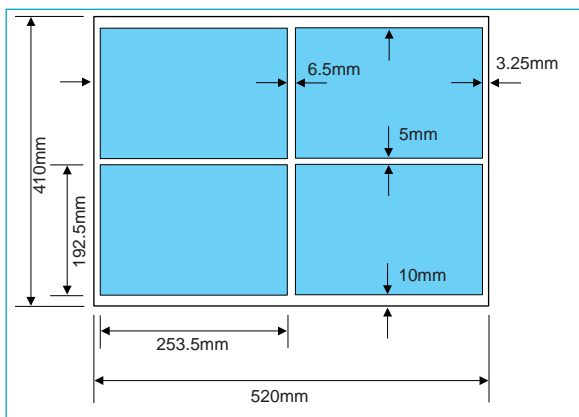


Fig. 6 Layout used for producing four 12.1" LCDs from 410 × 520mm sheet.

ing design that prevents dust from accumulating in the chamber and reduces flaws in the border area. Fig. 7 shows variations in film thickness at the substrate edge.

PATTERN ACCURACY. Several errors in dimensional accuracy at sheet edges can arise during the photolithography process: photoresist can thicken at the edges during the edge rinse process, warpage of the glass can cause temperature variations at the edges, and reflectivity of the substrate can drop due to reduced film thickness. We prevented thickening of the photoresist during edge rinse by designing the unit to exclude excess solvent. Low-stress conditions were used to minimize substrate warpage, and better temperature control was adopted for the bake phase. Fig. 8 shows the dimensional improvement we achieved.

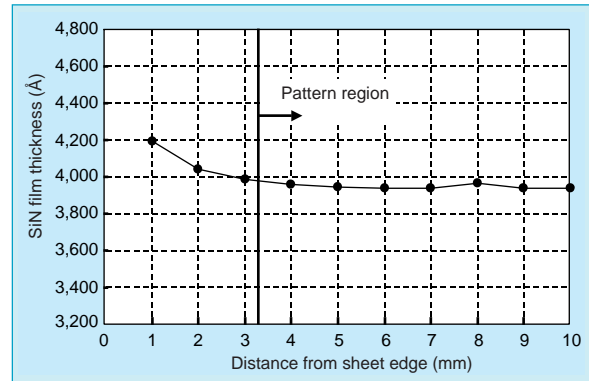


Fig. 7 CVD film thickness vs. distance from sheet edge.

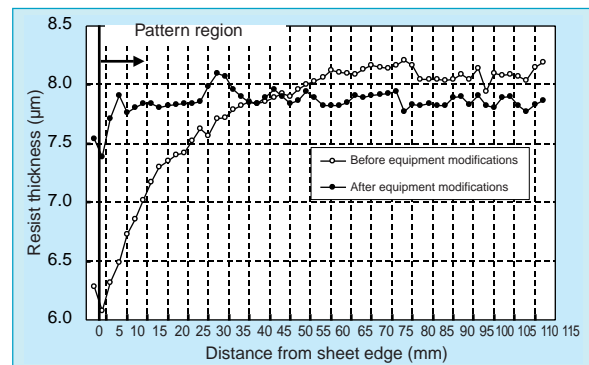


Fig. 8 Resist thickness vs. distance from sheet edge.

DEFECT CONTROL AT SUBSTRATE EDGES. Defect rates at the substrate edges greatly affect overall process yields. Fig. 9 shows defect rates as a function of distance from the substrate edge. The data was recorded during the line's second stage of development, prior to the introduction of automated equipment. Defects increased approaching the substrate edge following a logarithmic relationship. A systematic approach was used to reduce flaw incidence through equipment design, process parameter control and the use of a mass production ramp. These efforts, combined with the benefits of fully automated production, have improved yields above previous LCD lines.

Nearly two years have passed since mass production began at the Shisui Factory. As planned, the 12.1" SVGA panel is in full production and

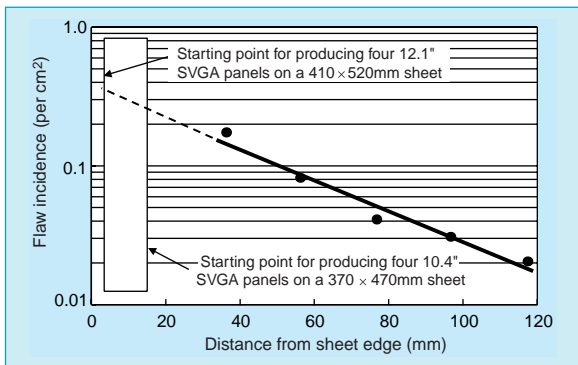


Fig. 9 Flaw incidence vs. distance from sheet edge after completion of second-phase construction.

a 15.1" XGA display entered mass production in the autumn of 1997. Our experience demonstrated that larger sheet sizes are not necessarily better. Rather, substrate size is best determined through scientific analysis of target products, development and cost of production equipment, production schedules, rationally balancing cost and technical advancement.

The use of full automation was also seriously debated. While automated handling would be an obvious target for cutting costs, total automation proved highly valuable, not only in reducing contamination, damage and dropped panels, but also in facilitating the analysis and resolution of quality problems, stabilizing yields and shortening construction time. The automated system readily adapts to changes in process parameters and work flow while dramatically reducing opportunities for human error. Especially noteworthy is the rapid failure analysis that became possible once the automated system was in place. The higher initial investment is justified by the longer life of LCD lines compared to semiconductor lines. Equipment may be replaced but modifications to clean room facilities, as seen in semiconductor lines, are relatively rare.

In setting up the Shisui Factory, the LCD Development Group was supported by numerous engineers with experience in the development and mass production of semiconductor devices,

equipment design and other relevant fields. LCD production has been considered to be quite different from semiconductor production, especially with regard to processing uniformity at substrate edges. In fact, many of the problems characteristic of LCD processing result from manufacturing equipment that has not been fine tuned like that for semiconductor processing. Achieving desired levels of throughput, operation duty and particulate control requires cooperation with equipment vendors. By having our process engineers and equipment designers work with vendors, we were able to identify key technical issues and resolve problems at an early stage, thereby supporting a rapid vertical ramp. We believe this approach will be even more important in future lines for larger substrate sizes. □

Static Electricity Control and Glass-Cutting Technique for Narrow Margins

by Takayuki Ohishi and Dr. Kazushi Haruna*

This article discusses two important developments Mitsubishi Electric has incorporated into the fabrication of its LCD panels: 1) measures for controlling static electricity, and 2) a technique for attaining narrow margins when cutting substrate glass.

Background

In addition to securing sufficient machining precision at substrate edges in array processes (described elsewhere in this issue), the ability to obtain four 12.1" panels from 410 × 520mm substrates depends on the control of static electricity in the array and panel processes, and also on the technique used to cut the substrate glass to obtain narrow margins during LCD panel fabrication.

We have developed a prototype two-dimensional electrostatic mapping system to detect static charge across the entire substrate surface, up to the glass edges, and employed it at the Shisui Factory. Using this system, we examined measures to prevent static charge in each piece of manufacturing equipment from the time of line startup.

In LCD panel manufacturing processes, after applying color filters at specified intervals to a substrate in the batch processing of four panels, and before the liquid-crystal material is injected, substrates must be cut into separate cells. Cutting conditions were determined empirically or based on experience in the past, but we constructed a model for numerical analysis using the finite element method (FEM) and then evaluated process conditions numerically. As a result, we were able to efficiently determine scribe-break conditions for narrow-margin cutting, and succeeded in the problem-free startup of panel processes.

Measures to Control Static Electricity

CONTROLLING CHARGE BUILDUP. A fieldmeter is normally used to measure electric potential in one of two ways. In the first, static electricity is identified phenomenologically with the electric potential, and the potential is measured in volts. In the second, static electricity is identified with the electric charge itself, and

measurements are performed to determine the distribution of accumulated charge over the area of the glass substrate. In order to obtain pointers for measures to control charge buildup, we opted for the second of these approaches.

When static charge accumulates over the entire glass substrate, the total amount of charge is considerable and the potential of the glass substrate as a whole is correspondingly high; this may possibly cause malfunctions in an external substrate sensor, for instance, due to local static discharge or other phenomena. On the other hand, when static buildup is local, the surface area involved is small compared with the entire glass substrate, and the amount of charge is correspondingly small. However, precisely because the buildup is local in nature, an electric field appears along the substrate surface and, depending on the intensity of this field, discharge may occur across the electrodes of elements on the substrate, possibly causing elements to be destroyed.

At the Shisui Factory, policy calls for measures to be taken when static electricity is detected, even if local in nature, at the time of startup of manufacturing equipment.

ELECTROSTATIC MAPPING SYSTEM. In order to measure static electricity in the form of electric charge, measurements must be performed with a constant electrostatic capacity (distance) between the glass substrate and a grounded surface. We therefore developed the prototype electrostatic mapping system shown in Fig. 1. In this system,



Fig. 1 Electrostatic mapping system.

Takayuki Ohishi is with Advanced Display Inc. and Dr. Kazushi Haruna the Advanced Technology R & D Center.

insulating spacers of fixed thickness are placed on a metal stage, and the glass substrate is placed on the spacers to perform measurements.

Several fieldmeter probes are positioned at equal intervals; by scanning them in X and Y directions within the glass substrate surface, the in-plane distribution of charge over the entire glass substrate surface can be measured in detail, without missing any areas of local charge buildup.

Actual Example of Measures to Control Static Charge

After processing a glass substrate using manufacturing equipment, static electricity measurements yielded the results shown in Fig. 2.

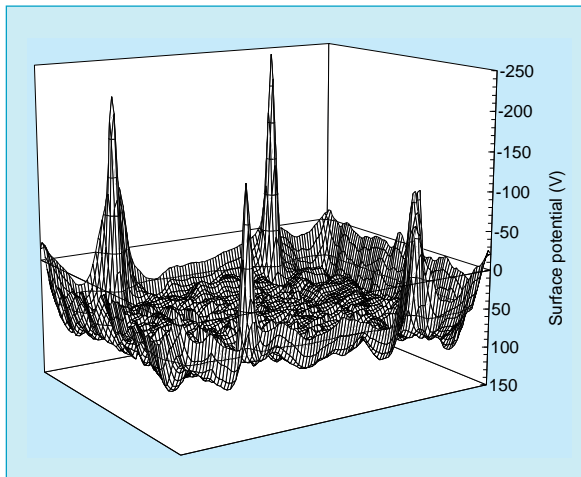


Fig. 2 Partial charge-up of glass substrate by one manufacturing apparatus.

On comparing the locations of charge buildup with the construction of the manufacturing equipment, it was discovered that certain parts in the equipment exist at positions corresponding to the areas of charge buildup, and that contact between these parts and the glass substrate gives rise to static electricity. By treating these parts, the occurrence of local charge buildup like that observed initially was suppressed (see Fig. 3).

Further, as the result of removing glass substrate from the production processes and performing static charge measurements, charge buildup was discovered along the short edges of the substrate. Based on the position of this charge and the circumstances of contact with the glass substrate in the production line, the transport rollers were identified as the origin of the charge buildup. Next, one side of the rollers was subjected to antistatic measures and measurements performed; the results of which appear in Fig. 4. Charge buildup continued on the

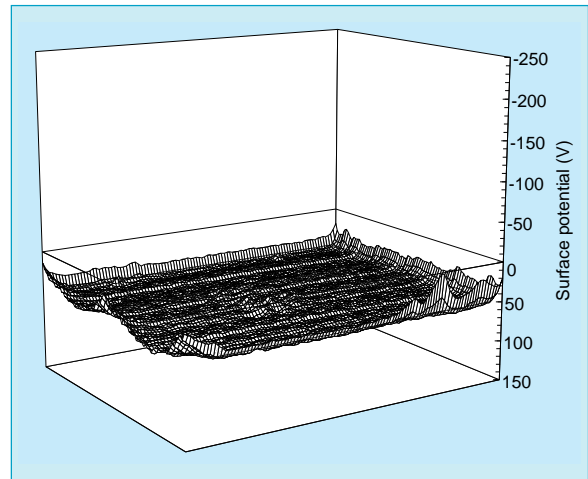


Fig. 3 Surface potential of glass substrate under electrostatic control.

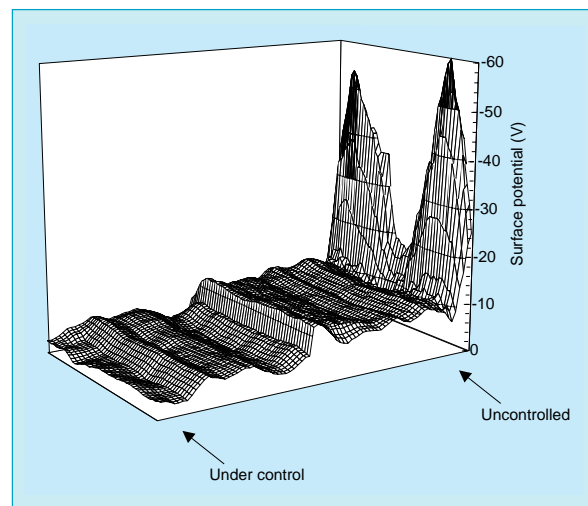


Fig. 4 Charge-up of glass substrate by conveyor roller and effect of electrostatic control.

side with the untreated rollers, whereas no charge buildup was observed on the side of the treated rollers. By employing this treatment throughout, it was possible to control the static electricity due to transport rollers.

Freedom from Ionizer-Dependent Methods

When it is impossible to determine the details of static electricity, it can be difficult to discover the cause of static charge buildup. At such times, measures to control static electricity tend to be of the ionizer-dependent type—typically “spraying with an ionizer to control charge buildup.” As a result, many ionizers may actually serve no useful purpose, and their use should be controlled.

At the Shisui Factory, since it has become possible to determine the minute details of static electricity appearing on glass substrates, necessary ionizers can now be distinguished

from those that are not and the latter eliminated. In addition, by examining static electricity in the form of electric charge and developing techniques for suppressing the occurrence of charge itself within various manufacturing equipment, some previously necessary ionizers have been eliminated.

Techniques for Glass-Cutting of Narrow Margins

In glass-cutting processes the “scribe-break” method is employed, in which a crack (scribe) is introduced between panels and the back surface is then tapped to cut (break) the glass. The scribe-break method does not use water or heat, generates little dust and is an excellent method for preventing product contamination; but as the scribing interval is decreased it becomes difficult to control the cutting process. This is because when panels are cut, several scribes normally exist surrounding a panel. But as panels increase in size, the interval between scribes decreases, and problems arise in which cracks spread in the neighborhood of a scribed area when the break is made. The conditions of the scribe-break method are established empirically, and limits and optimal conditions have remained unclear. We therefore used the finite element method (FEM) in a model for numerical analysis, and attempted to evaluate process conditions. If a method is established for the numerical analysis of scribe-break processes, not only can the number of experiments required be reduced, but the rapid elucidation of parameter limits and optimal conditions will be possible at minimal expense.

Analysis Model

When considering crack propagation during breakage as a problem in a plane, it can be represented as a combination of two modes—mode I, in which cracks separate from each other as they propagate, and mode II, in which cracks shift within the plane. That is, it is thought that crack propagation properties can be evaluated in terms of the stress intensity factor at the scribe tip calculated from the nodal displacement on the crack surface obtained from FEM stress analyses. Hence, our goal here is to calculate stress intensity factors for modes I and II (KI and KII, respectively).

Fig. 5 is a schematic diagram of the analysis model and boundary conditions. Plane strain elements are used in modeling the central area for cutting to obtain four panels. Scribes are taken to be cracks 0.1mm deep, and break positions are given as nodal forces calculated from the pressure that is applied to the cylinder of

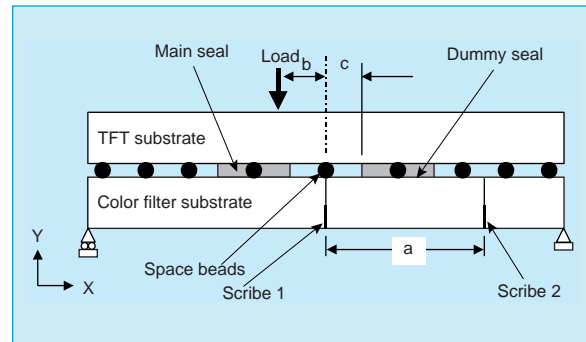


Fig. 5 Schematic and boundary condition of analysis model.

the cutting equipment. Spacer beads, which cover approximately 10% of the area, are modeled as beam elements with the equivalent stiffness. The effect of beads in the seal material was represented by material constants computed from the equivalent elasticity using the law of mixtures. Because it is determined by the panel size, the main seal position was taken to be constant; and the scribe intervals, load positions and dummy seal positions (denoted by a , b and c , respectively) were considered as shape factors in the cutting process. Initially, b and c were held constant and a was set at 3 mm; but the value varied in the range of 1mm, and the results of analyses were compared with experiments to evaluate the model validity. In experiments, satisfactory cutting was possible at scribe 1 for $a+1$ mm. But at a and $a-1$ mm, cracks propagated in unwanted directions toward the neighboring scribe 2, so cutting at scribe 1 was not possible.

Fig. 6 shows the relation of the scribe interval to KI and KII. For $a+1$ mm, KI is higher on the side of scribe 1. The stress intensity factor is a measure of the intensity of the stress field at the crack tip, and it is expected that the crack will propagate on the side of scribe 1. When using a and $a-1$ mm, KI is higher on the scribe 2 side, leading us to expect that crack propagation will occur on the scribe 2 side. On the other hand, the value of KII is nearly zero on the scribe 1 side, but is higher on the scribe 2 side as the scribe interval is reduced. Consequently, it is thought that the crack on the scribe 2 side is due to a mixture of mode I and mode II propagation. In order to obtain good-quality cuts in the scribe-break method, cracks must be due to pure mode-I propagation. Therefore, for a and $a-1$ mm, it is expected that the crack on the scribe 2 side will propagate in an unwanted direction. These predictions are in agreement with the previously mentioned experimental results; indicating the validity of the analysis model and the evaluation method employing stress intensity

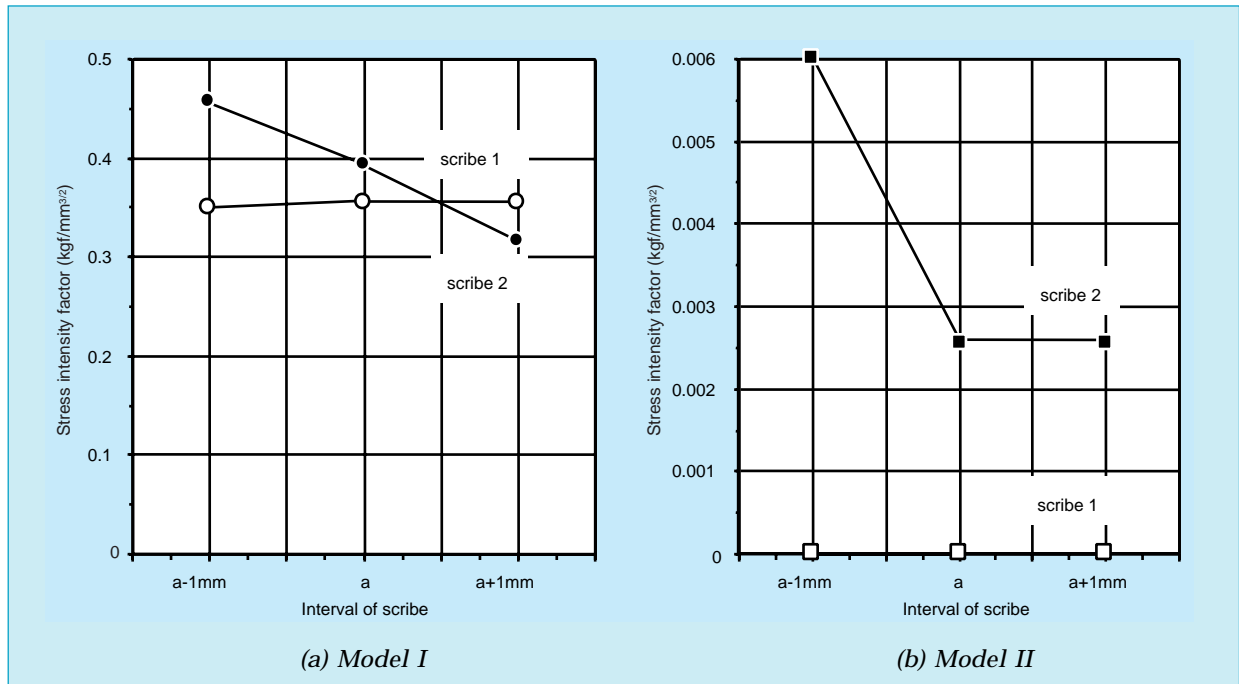


Fig. 6 Relationship between an interval of scribe and stress intensity factors in mode I and mode II.

factors as parameters. From the figure, we also see that the limiting scribe interval at which cutting is possible for these process conditions is a +0.5mm.

Effect of Various Factors on the Cutting Process

The validity of the analysis model was thus confirmed, and load position b and dummy seal position c were varied to determine changes in stress intensity factors. Scribe interval a was held constant. Fig. 7 shows the relation of b

and c to KI. Focusing on load position b, we see that shifting the load toward the main seal results in a lower KI value on the scribe 2 side, and cutting at scribe 1 is easier. This is probably because, by distancing the load position from scribe 2, deformation in the vicinity of scribe 2 is diminished. As for dummy seal position c, shifting the dummy seal toward scribe 2 is also effective in lowering the KI on the scribe 2 side. Transmission of the load placed on the scribe back surface to the substrate scribe side is thought to occur primarily via the seal material. Hence, by moving the dummy seal, which affects deformation in the vicinity of scribe 2, away from the load position, it should be possible to reduce the deformation near scribe 2.

The following were found to be effective for alleviating problems with unwanted crack propagation at the second scribe:

1. Placing the breaking load on the main seal side, and
2. Using a seal pattern in which the dummy seal is placed as close as possible to the second scribe.

A combination of accurate measurements of electrostatic charge distributions and mathematical analysis of crack propagation enabled the identification of critical parameters and their optimum values for smooth and efficient startup of LCD production lines. □

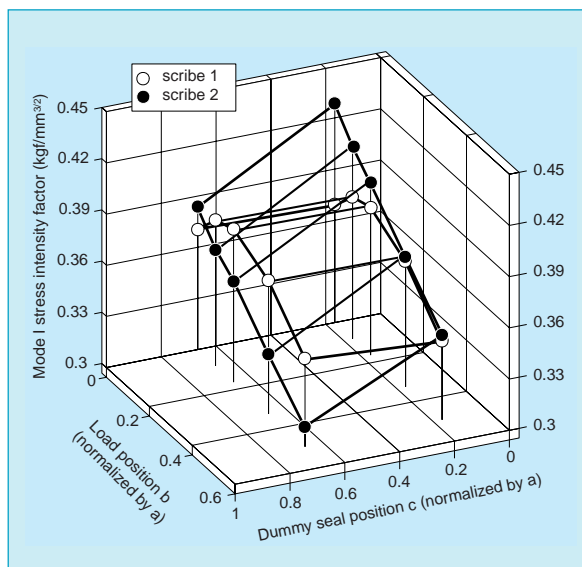


Fig. 7 Effect of load and dummy seal positions.

Design Technologies for Low-EMI Notebook Personal Computers

by Dr. Eishi Gofuku and Shinji Tanabe*

Advances in computer science and hardware in recent years have made possible three-dimensional simulations of electromagnetic interference (EMI) phenomena. We at Mitsubishi Electric have developed a simulator and are now utilizing it to analyze the relationship of radiation intensity to current densities in printed circuit boards (PCBs) and the structure of liquid-crystal displays (LCDs); the results of which are applied to product design. This represents a new direction for research.

In this paper, we describe LCD designs to reduce emission noise, drawing on measurement results obtained using a three-dimensional electromagnetic field simulator (MAGNA/EMI) based on a finite element method and developed jointly by Mitsubishi Electric's Advanced Technology R&D Center and the CRC Research Institute.

Background

The sizes of LCD devices have become larger and the picture quality has improved. This has led thin-film transistor (TFT)-LCDs to dominate as the display for "notebook" personal computers (PCs). Since high-speed digital processing is necessary for image display, the radio-frequency components of such signals are, to a greater or lesser extent, radiated away from the display as an RF noise.

Standards (tolerances) have been established in order to prevent this undesirable radiation. Nearly all such standards conform to or are based on international standards established by the International Special Committee on Radio Interference (CISPR). CISPR 22 (2nd edition) is, in effect, an international passport for electronic products where electromagnetic emissions are concerned; for manufacturers of electronic equipment, meeting the standards and regulations for EMI is absolutely essential if their products are to have free entry to overseas markets.

Electromagnetic Field Analysis Using the Finite Element Method

FEATURES OF EMI IN LCD DISPLAYS: The sizes of PCs are nearly the same length as half of the wavelength at 200 or 300MHz, thus causing EMI

noise amplitude resonance.

As the bezels of LCDs are made smaller and the area available for PCBs is reduced, the power-supply impedance of the circuit board rises and high-speed switching noise from semiconductor devices tends to be emitted as common-mode noise.

Because the power and signals are supplied to the LCD via a PC, power is unstable as compared to that distributed to devices within the PC itself. Moreover, the cable connecting the PC and the LCD acts as a radiating antenna.

In addition to examining transmission paths, analyses of the above phenomena must also include: (1) consideration of electromagnetic emissions from the system comprising PCBs, cables and an enclosure; (2) treatment of the power supply and ground as antennae with finite impedance, rather than as ideal perfect conductors; and (3) consideration of actual cable shapes.

Advantages of Finite Element Method Analysis

There are a number of advantages in applying a finite element method. These include: (1) the permittivity, permeability, conductivity, and other actual physical parameters in the analysis; (2) the three-dimensional analysis for approximating the actual geometry; (3) solutions without approximating to problems at intermediate distances, neither "near" or "far" field; and (4) automatic inclusion of electromagnetic wave radiation, reflection, refraction, resonance, and other physical phenomena.

Because our finite element method uses sparse symmetric matrices, the method is superior to other analysis techniques (such as the method of moments) with respect to calculation speed and memory requirements. The MAGNA/EMI simulator adopts a unique FEM algorithm; making it possible to analyze entire equipment systems.

Relation of PCB Position to Noise Emission

NOISE EMISSION FROM PC SYSTEMS EQUIPPED WITH LCDs: PCBs on which ASICs (timing controllers) have been mounted to perform high-

*Dr. Eishi Gofuku is with the LCD Marketing Division and Shinji Tanabe the Advanced Technology R & D Center.

speed switching can become a source of electromagnetic radiation, driven by a common-mode input of the entire power-supply subsystem. For instance, half of the wavelength ($\lambda/2$) at 250 MHz is about 63 cm, so that with the PCB supplying power, the metal frame of the LCD or the PC housing can emit radiation as a half-wavelength resonance antenna (Fig. 1).

Even when countermeasures are introduced at the PCB level, if the feedback length to the ground of the noise current matches the resonant length for a certain frequency, the radiation intensity jumps drastically, and measures to remedy symptoms become problematic at or near that frequency.

Relation of PCB Position to Electromagnetic Emission

The following three types of analyses of EMI from PC systems were performed using a three-dimensional finite element method:

1. PCB mounted at the lower part of the LCD,
2. PCB mounted at the upper part of the LCD, and
3. PCB mounted at the upper part of the LCD, and with a metal shielding plate on the back surface of the LCD.

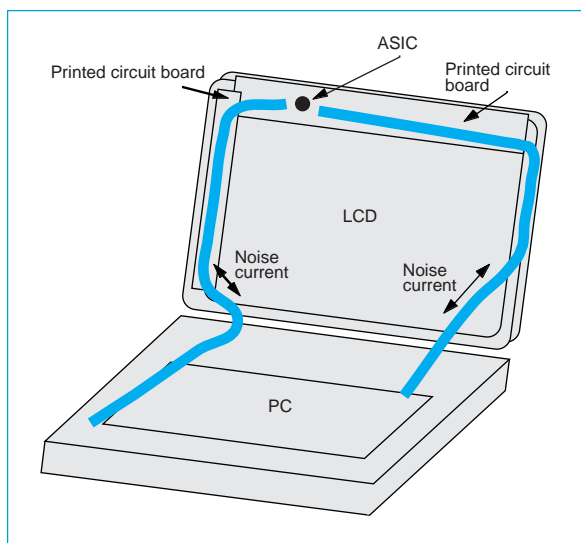


Fig. 1 Noise current paths.

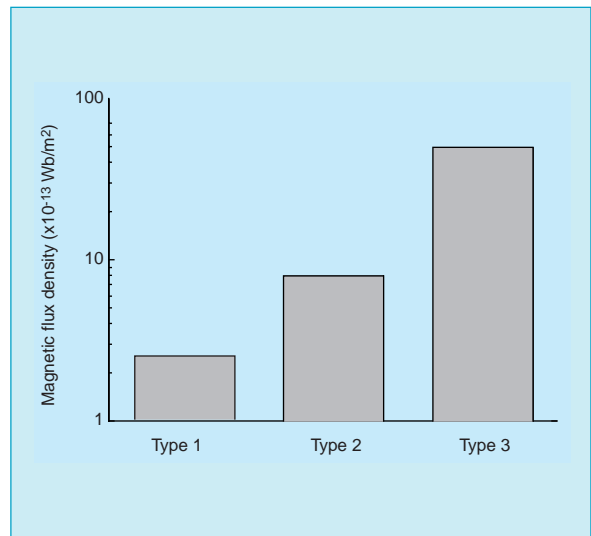


Fig. 2 Electromagnetic radiation from different LCD types.

In calculations, we assumed that the PCB is bouncing at $\pm 1V$, and that electromagnetic radiation is emitted from the whole of the PCB. Emissions for each type of system are compared in Fig. 2, which shows the magnetic field strength for each case (magnetic field strengths are shown because electric field strength values are affected by static electricity fields). When a PCB is mounted on the upper part of the LCD, noise currents flow to the ground via the LCD metal frame, which has a high specific impedance. Here, the metal frame becomes a kind of antenna. When a metal plate or other material is placed on the back surface of the LCD, the gap between the LCD and the metal plate changes the impedance of the noise current path, particularly in the vertical direction. This is one factor that generates radiation. By mounting the PCB at the bottom of the LCD, such phenomena are suppressed.

EMI from PCBs

ANALYSIS OF NOISE CURRENT COMPONENTS IN A PCB: The ASIC mounted on the PCB, with its relatively high impedance, also acts as a source of common-mode EMI. When the ASIC is “on,” penetrating current spikes flow between the power supply and the ground. These currents

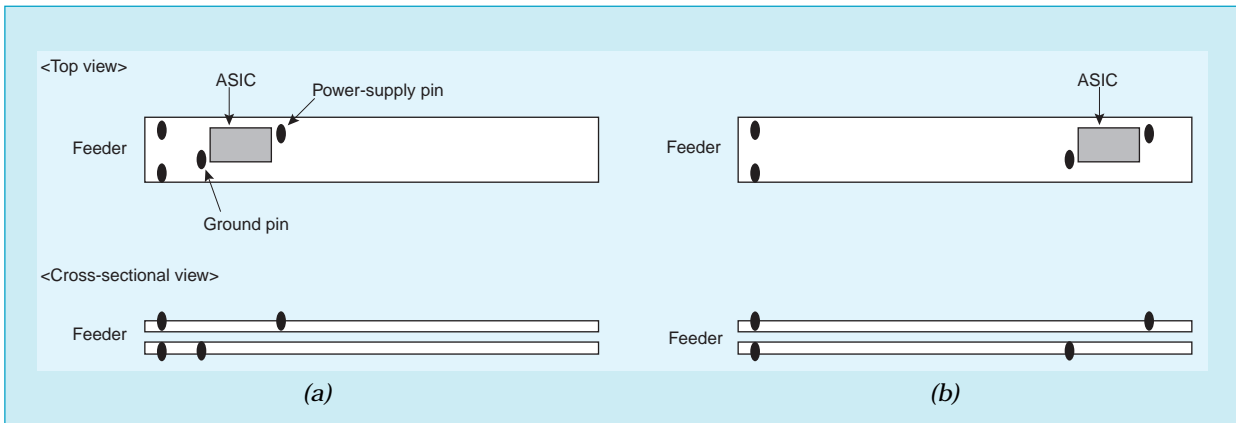


Fig. 3 Analysis and measurement models.

bounce the voltage level of the PCB at radio frequencies. Because of the bouncing, the power supply and ground are in phase, and the entire PCB acts as a kind of patch antenna to radiate considerable intensities of electromagnetic noise. This phenomenon is known as “ground bouncing” or as “delta-I noise.”

ANALYSIS AND MEASUREMENTS OF EMI FROM PCBs: The energy of the noise is propagated as transverse electromagnetic (TEM) waves between Cu layers in the PCB. It is different from low-frequency currents. Fig. 3 shows a model used in the analysis and measurements. In (a) the ASIC is positioned on the side of the power supply for the PCB; and in (b) it is positioned on the opposite side. Fig. 4 shows the results of an analysis of both cases. At radio frequencies, currents are concentrated at the edges of the PCB. Fig. 5 shows actual measurement results, comparing EMI intensities at 3m separation. In the former case, the side opposite the ASIC “floats” and the PCB as a whole acts as an antenna, so that radiation is increased. The frame ground is mounted on both edges of the PCB so that it does not become a radiating antenna.

Radiation from Cables

The cable connecting the PC to the LCD is another source of radiation. Here, we discuss the flexible cables (FPCs) that are typically used. In order to reduce radiation from such cables,

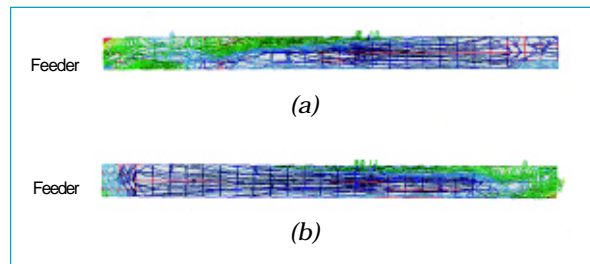


Fig. 4 Current distributions within a printed circuit board.

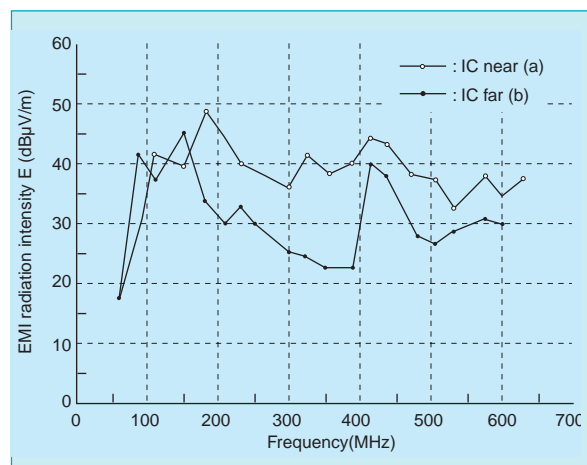


Fig. 5 Differences in EMI radiation depending on ASIC position in the printed circuit board.

the first priority is to match the overall impedance in the circuit. As Fig. 6 shows, an in-plane

structure (a) has small capacitive coupling, and therefore a high specific impedance. A two-layer

microstrip structure (b) can be designed to have a specific impedance nearly equal to that of the

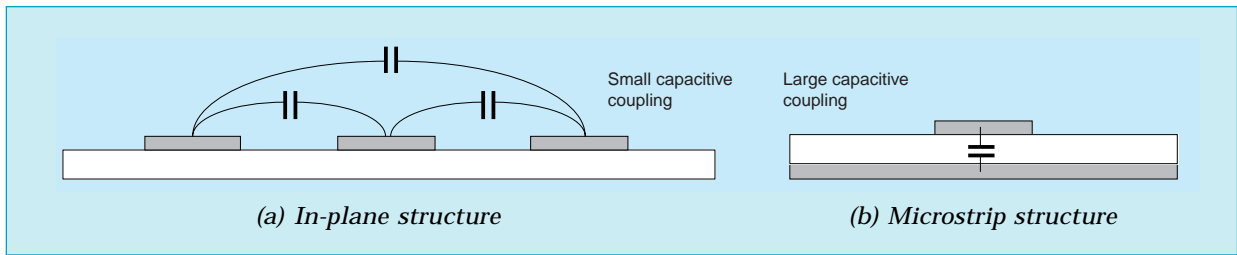


Fig. 6 Capacitive coupling of in-plane and microstrip structures.

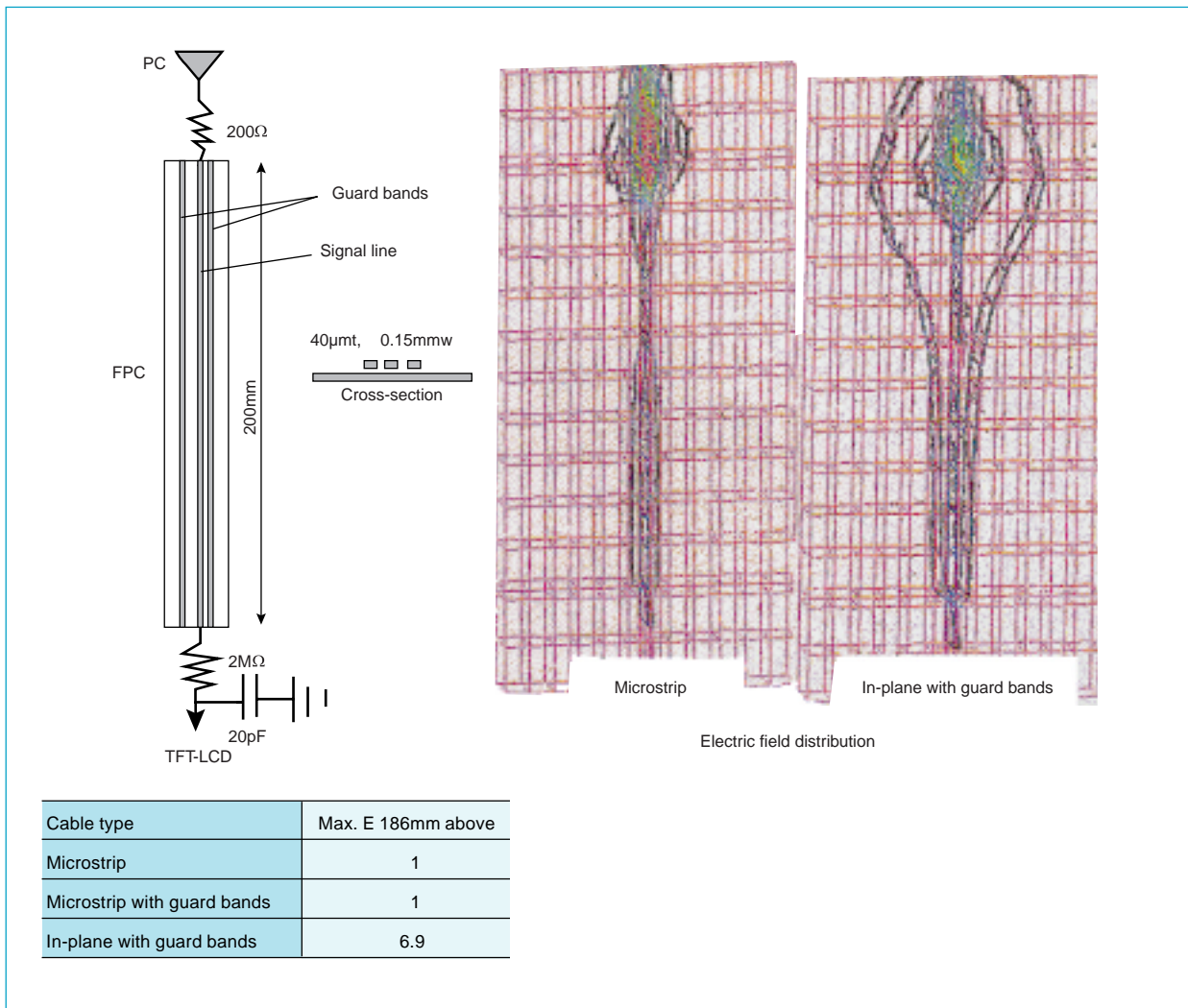


Fig. 7 EMI radiation from a flat cable with microstrip and in-plane structures (calculated).

transmission path.

Fig. 7(a) and (b) present the calculated results for the EMI radiation from an in-plane structure (with one Cu layer and guard bands on both sides), and from a microstrip structure (with two Cu layers, the lower of which is a grounded layer), respectively. Fig. 8 shows the results of measurements of the electric field intensity at a distance of 3m. Measurements and calculations are in good agreement. The radiation level from a microstrip-structure FPC is smaller than that from an in-plane FPC by less than 10dB. If the cable employs a three-layer strip structure, the radiation level can be reduced, but the cable itself becomes harder to bend. The optimum structure must be chosen with consideration being given to the constraints and conditions imposed by necessary PC functions.

It is said that measures to control EMI in electronic equipment have all remained at the PCB level. In fact, EMI must be evaluated for the entire system; even if the noise of individual PCBs in an LCD is reduced, it is difficult to tell

in advance how much noise will be generated when the assembly is incorporated into a notebook computer. Here, we stress that the structure and electrical connections of the LCD as a whole are important factors to reduce total radiation noise. Using techniques for electromagnetic field analysis in three-dimensional space, electromagnetic radiation from LCDs incorporated into computer systems can be predicted quantitatively. LCD structures are encountering an increasing number of constraints as LCDs become thinner and lighter. But basic measures to counter EMI can be incorporated at early stages in the design of PCs and LCDs, rather than relying solely on design features to control EMI at the PCB level.

Advanced Display Inc. has utilized the above analysis techniques in designing all its products, and has implemented measures at manufacturing plants to ensure that products pass all EMI regulations. □

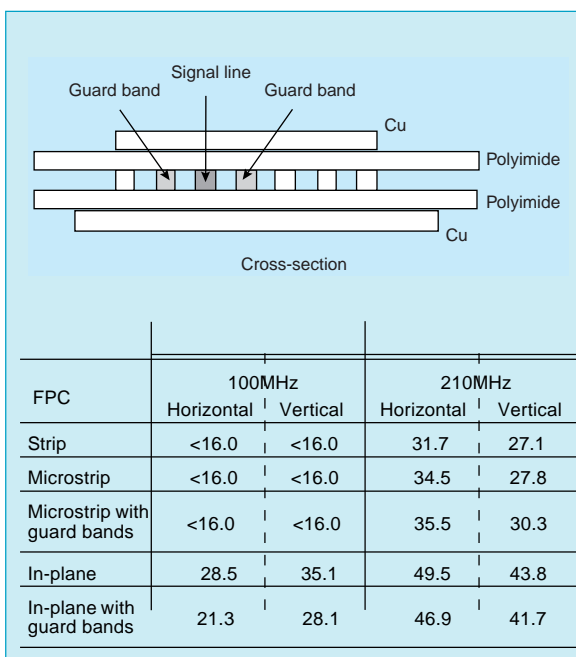


Fig. 8 EMI radiation from a flat cable with microstrip and in-plane structures (measured).

An Optimum Pixel Light-Shield Pattern Design for TFT-LCDs

by Shigeru Yachi and Yasuo Fujita*

In this article we discuss the design of shield patterns near pixel edges, which are vital to the image quality of thin-film transistor (TFT) liquid-crystal displays (LCDs), including a newly adopted design concept for shielding light leaking in oblique viewing directions. This design was employed in the development of a 14.2-inch XGA TFT-LCD to achieve satisfactory optical performance.

Misalignment at Pixel Edges and Light Leakage

Each pixel can be driven independently in TFT-LCDs, enabling high contrast and excellent image quality. However, light leakage at the edges of the pixels can occur due to misalignment arising from the lateral electric field. Effective shielding of this leakage is essential for excellent image quality.

Fig. 1 is a planar diagram of a single TFT-LCD pixel; and Fig. 2 is a cross-section of a cell along the line A-A' in Fig. 1. In TFT-LCDs, the “on” and “off” signals applied by the TFTs to the gate bus-line are controlled to selectively apply the video signal voltage of the source bus-line to the pixel electrodes. This means that the electric field intensity in the perpendicular direction between the pixel electrode and the opposing electrode is controlled by the video

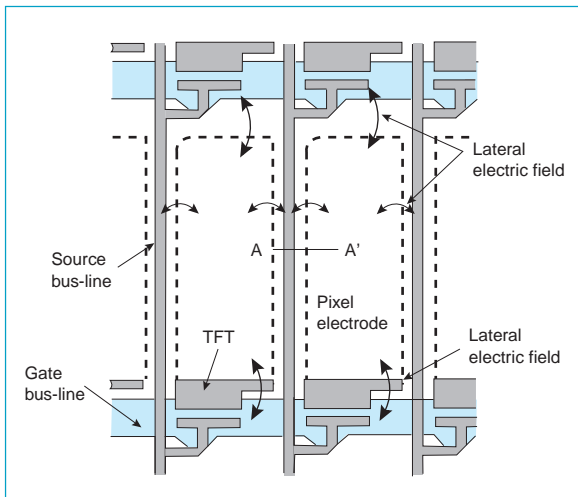


Fig. 1 Top view of TFT-LCD pixel.

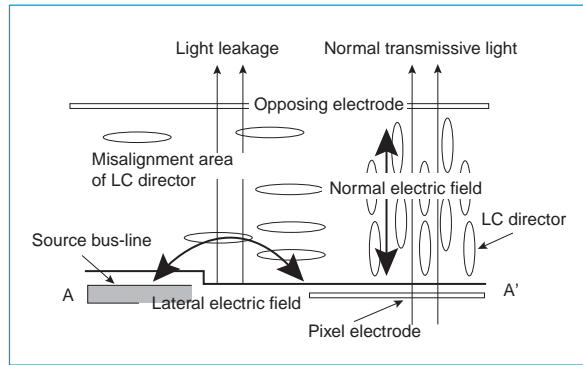


Fig. 2 Cross-sectional view of TFT-LCD cell.

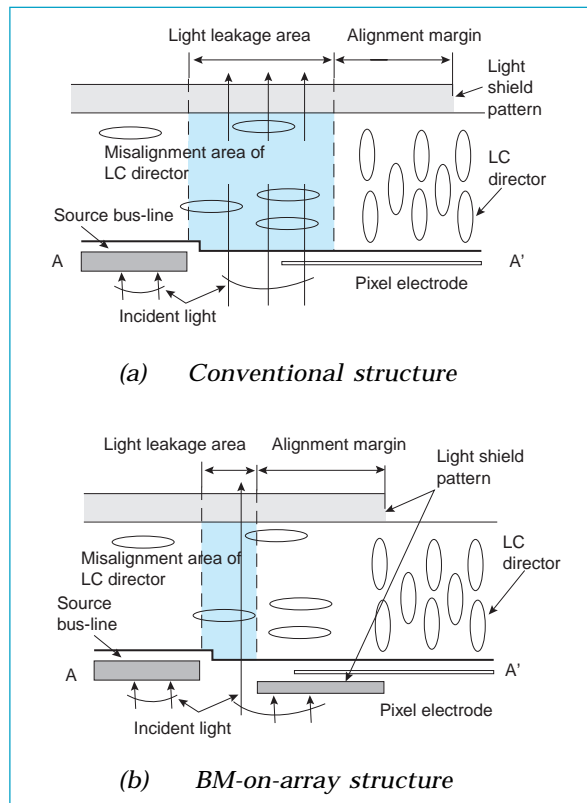


Fig. 3 Light-shield structure and design parameters.

signal voltage. The arrangement (hereafter “alignment”) of liquid-crystal molecules is controlled by this perpendicular-direction electric field, as a result of which the intensity of light transmitted at the pixel is modified.

*Shigeru Yachi and Yasuo Fujita are with Advanced Display Inc.

As is clear from the figure, the appearance of a lateral electric field due to the gate and source signals in the vicinity of the pixel electrode is unavoidable. Because liquid-crystal molecules tend to align themselves in the direction of this electric field, misalignment results—liquid-crystal molecular alignment differs from the center of the pixel. As explained above, the alignment of liquid-crystal molecules is controlled in order to regulate light transmission in an LCD; hence, even in an area of the display which should be black, light leakage occurs owing to this misalignment. If this leakage is not shielded, contrast is degraded and problems with image quality arise.

Shielding Pattern Design

Methods for shielding light leaking from pixel edges may be broadly divided into techniques in which a light-shielding layer is formed only on the opposing substrate (conventional methods) and those in which light-shielding patterns are formed both on the opposing substrate and the TFT substrate (the BM-on-array method) (Fig. 3).

Design parameters for light-shielding patterns on the opposing substrate are as follows:

- Light leakage region,
- Pattern tolerance on the TFT substrate,
- Pattern tolerance on the opposing substrate, and
- Precision of alignment of TFT and opposing substrates.

Among these, the light leakage region and the precision with which the TFT and opposing substrates are aligned are parameters of especially great design importance. The shielding pattern design value is approximated as follows:

$$\begin{aligned} & \text{(shielding pattern design value)} = \\ & \text{(light shielded in leakage regions)} + \\ & \text{(precision of alignment of TFT substrate and} \\ & \text{opposing substrate)} \dots\dots\dots \text{Eq. (1)} \end{aligned}$$

In recent years, demand has redoubled for TFT-LCDs with low power consumption, particularly for use in notebook computers, and improvement of the transmission characteristics of LCD panels has become essential. One means to achieve this is to raise the pixel aperture ratio; here, the problem is how to reduce the shielding pattern design value. In a BM-on-array structure, reduction of the light leakage region in Eq. (1) is possible using a shielding pattern with good precision on the TFT substrate; this is an effective means of increasing

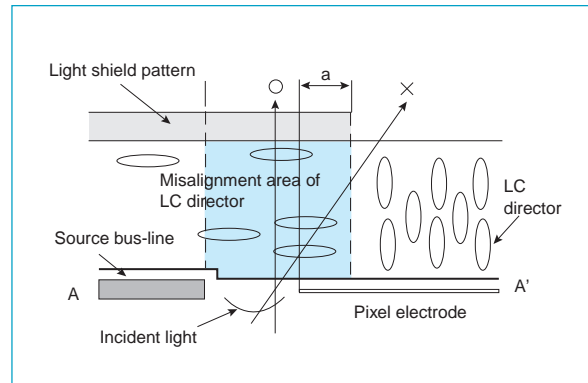


Fig. 4 Light leakage in oblique incidence.

the aperture ratio.

Let us next consider the amount of shielding in the region of light leakage, which accounts for a large amount of shielding. Fig. 4 is a schematic diagram intended to explain light shielding using conventional techniques; the amount of shielding is defined by the overlap with pixel electrodes. Here, it is clear that light advancing in the perpendicular direction in the misalignment region is shielded, but light in oblique directions is transmitted. This oblique leakage has an evident effect on the viewing angle characteristics of the display and other aspects of display quality when viewed at oblique angles. On the other hand, if the shielding amount is set too large, the aperture ratio (i.e., display brightness) suffers. Thus a tradeoff is involved, and it is important that the shielding amount be optimized. A quantitative evaluation of the effect of light leakage in oblique directions is essential to such optimization, but there have not yet been any reports on this problem.

At Mitsubishi Electric, simulations and experiments have been conducted to evaluate the effect of this oblique light leakage. As one example of the results obtained, Fig. 5 shows the shielding amount (overlap *a*) and the contrast, with the viewing angle varied as a parameter (in a BM-on-array design, the shielding amount was defined as the overlap with the shielding pattern on the TFT substrate). The figure shows that the smaller the shielding, the poorer the characteristics. For current screen sizes (from 12" to 15" or so), it should be sufficient to consider viewing angles up to about 30°. At the latter angle, it was found that shielding (overlap) must be expanded by 2 to 3µm.

Application to 14.2-inch XGA TFT-LCDs

A 14.2-inch XGA-resolution TFT-LCD was developed incorporating the shielding design concepts described above to prevent light leakage

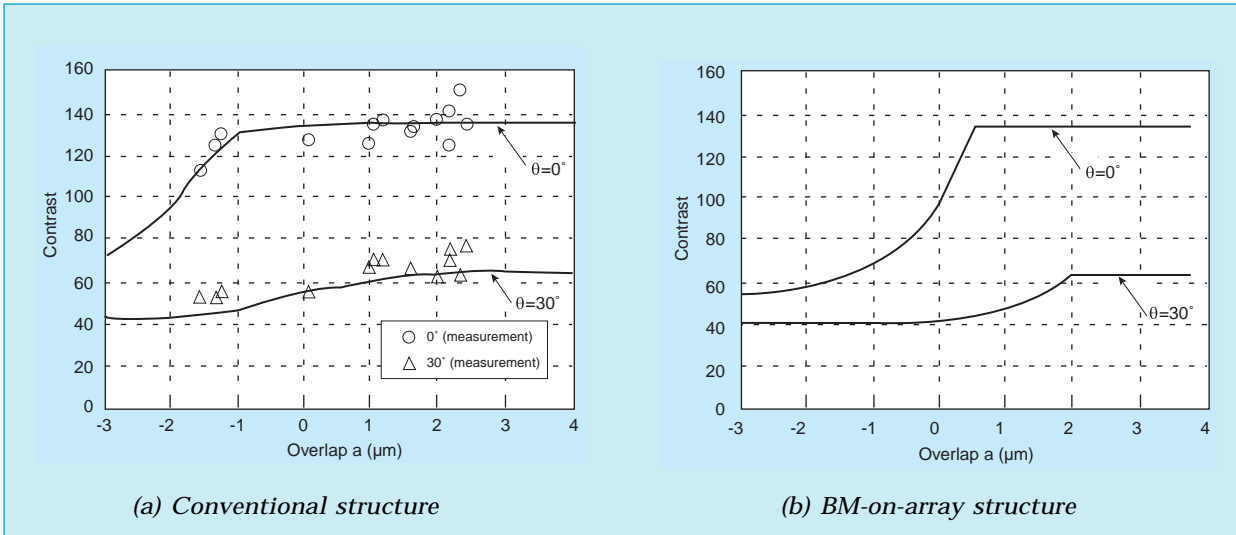


Fig. 5 Relationship between contrast and overlap a.

Table 1 Specification of 14.2-inch XGA TFT-LCD

Pixel number	1,024 × 768
Pixel pitch	0.28 × 0.28mm
Display size	288.8 × 216.6mm
Module size	303.0 × 230.5 × 9.0mm
Weight	790g
Power dissipation	4.5W without inverter loss
Luminance	70cd/m ²
Contrast ratio	150:1
Color number	260,000 colors
Backlight tube	CCFL × 1
Input voltage	3.3V

in oblique viewing directions. This display was developed for use in “mega-notebook” computers and desktop LCD monitors; it features a small bezel, thin shape, and the ability to display 260,000 colors. By optimizing the light-shielding structure, excellent viewing-angle characteristics were achieved, with the contrast remaining at 50:1 even at a 30° viewing angle. Specifications of the 14.2" XGA TFT-LCD appear in Table 1; and an external view of the display module is shown in Fig. 6.

Despite the inherently high contrast, excellent response and wide viewing angle of TFT-LCDs, they have inherent problems of light leakage that reduce their performance when viewed at oblique angles. This work shows how conflicting requirements can be reconciled and image viewing improved in a 14.2" XGA TFT-LCD. □

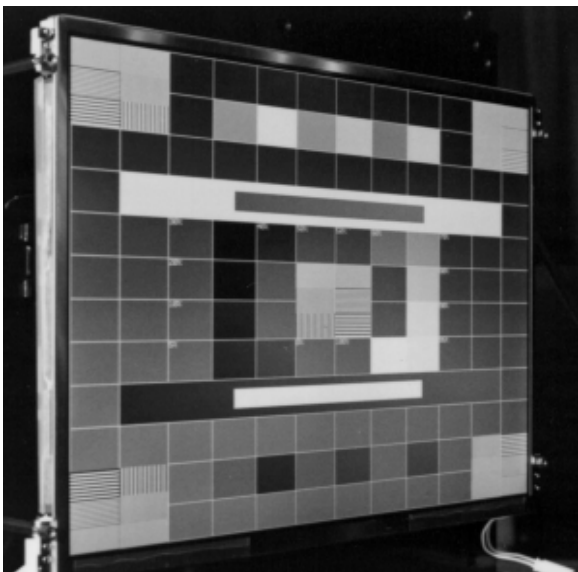


Fig. 6 14.2-inch XGA TFT-LCD module.

An LCD with a Wide Viewing Angle for PC Monitor Applications

by Shin Tahata and Masaya Mizunuma*

By using the recently proposed in-plane switching (IPS) mode, Mitsubishi Electric has developed a 15.1" XGA (1,024 × 768 pixel) liquid-crystal display (LCD) monitor with a wide viewing angle. This report describes the technologies introduced during development and their impact on display characteristics.

Operating Principles of IPS-Mode LCDs

IPS-mode displays offer a much wider range of viewing angles than twisted-nematic (TN) mode displays.

Fig. 1(a) and (b) illustrate the operating principles of an IPS-mode LCD panel versus those of the popular TN-mode panel design. Fig. 1(c) and (d) show the apparent birefringence(Δn) as a function of the viewing angle.

The IPS mode uses a pair of interdigital electrodes placed parallel to the x - y plane(Fig. 1a). E , an electric field in the x - y plane, is applied to the interdigital electrodes, causing liquid-crystal molecules initially arranged along the y axis to reorient themselves along the x axis. IPS-mode displays use this change in optical axis to switch pixels off and on. Looking at the liquid-crystal molecule from any direction, the apparent birefringence is nearly identical, Fig. 1(c). A display based on this principle will look relatively constant over a wide range of viewing angles.

In the TN mode, electrodes are placed above and below the z axis, Fig. 1(b), and the electric field is applied in the z -axis direction. This causes the liquid-crystal molecules to change from their initial orientation in the x - y plane and align themselves with the z axis. When the molecules stand up like this, the apparent birefringence varies greatly with the viewing angle, Fig. 1(d). This means that the display will only look right over a narrow range of viewing angles.

Panel Configuration

INFLUENCE OF METALIZATION ON OPPOSING SUBSTRATE. To achieve optimum pixel drive characteristics in the IPS mode, the electric field between the interdigital electrode pair should be as close as possible to parallel to the substrate plane. We performed a computer simula-

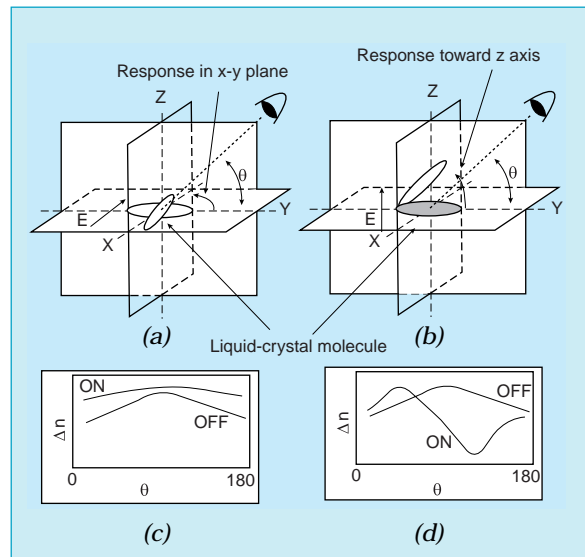


Fig. 1 Operating principles of TN and IPS-mode displays.

tion to determine the effects of using an opposing substrate with a conductive layer on the field configuration. Fig. 2 shows isopotential lines around the interdigital electrodes in devices with coated and uncoated opposing substrates. The electrode equalizes the voltage of the opposing substrate resulting in sloped isopotential lines, Fig. 2(a). However, the isopotential lines are nearly parallel to the substrate plane with an uncoated opposing substrate, Fig. 2(b), leading us to choose the uncoated design.

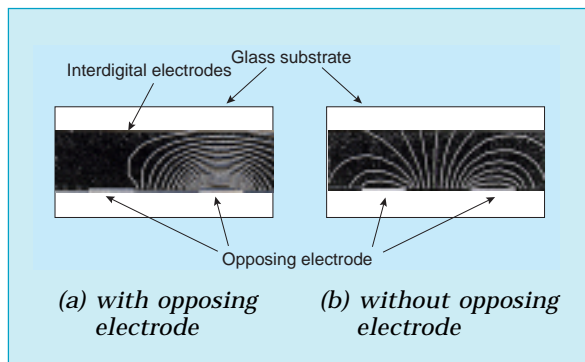


Fig. 2 Isopotential lines computed for interdigital electrodes.

*Shin Tahata is with the Advanced Technology R&D Center and Masaya Mizunuma with Advanced Display Inc.

PANEL GAP EFFECTS. Due to the different operating principles involved, the optimum panel gap for IPS-mode displays differs from the $4.5\mu\text{m}$ gap typical for TN displays. Fig. 3 shows drive voltage dependence on panel gap, and Fig. 4 response time *versus* panel gap. Fig. 5 shows the color coordinates of the transmitted light at various panel gaps.

Fig. 3 shows that wider panel gaps require a lower drive voltage. When the gap is narrow, in-plane movement of the liquid-crystal molecules that occupy the gap is significantly constrained by anchoring of the boundary layer, requiring a higher drive voltage. Conversely, a wider gap reduces this effect, lowering the driver voltage.

Fig. 4 shows that a narrow panel gap results in a faster display response for both rise time (τ_R) and decay time (τ_D). At the $4.5\mu\text{m}$ gap of a typical TN-mode display, the sum of the rise and decay response exceeds 100ms, while a gap narrower than $4\mu\text{m}$ results in a fast response suitable for personal computer (PC) display monitor applications. Another factor pointing toward use of a narrower panel gap is the yellow bias that occurs at larger panel gaps (Fig. 5).

LIQUID-CRYSTAL MATERIAL. IPS-mode devices respond to the electric field between the interdigital electrodes, so use of a liquid-crystal material that responds to weak electric fields will allow greater space between the interdigital electrodes. This increases the display aperture ratio—the proportion of the pixel area that allows light to pass—and leads to a brighter display.

To maximize the electric field response of the display, we therefore investigated liquid-crystal materials having large dielectric anisotropy. When this dielectric anisotropy is large, however, the material attracts impurities, leading to lower resistivity, lower holding ratio and increased drive voltages. We therefore selected a fluorinated liquid-crystal compound that is substantially immune to this kind of degradation.

ALIGNMENT LAYER MATERIAL. An alignment layer material with minimum pretilt angle is desirable since the wide viewing angle range of IPS-mode displays originates in the switching of liquid-crystal molecules in the plane of the panel. We tested many kinds of alignment layer materials, and found one with a pretilt angle of about 1° that stabilizes the alignment characteristics of the liquid crystals.

POLARIZER. When we fabricated IPS-mode displays without a conductive layer on the oppos-

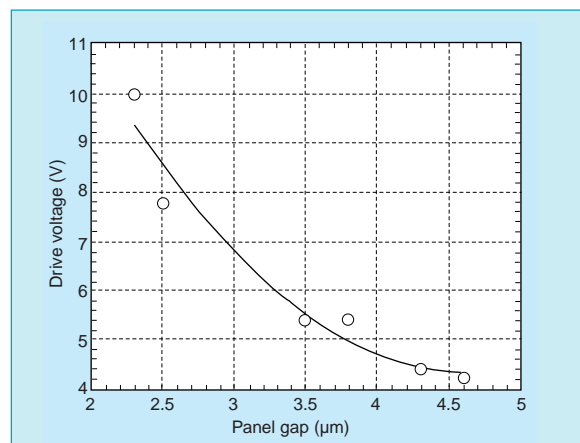


Fig. 3 Drive voltage vs. panel gap at $10\mu\text{m}$ electrode spacing.

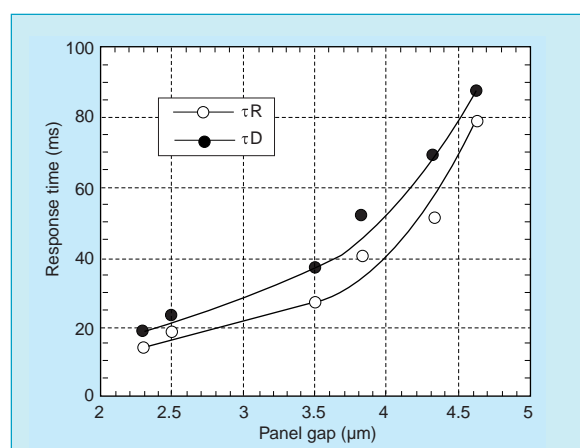


Fig. 4 Response time vs. panel gap at $10\mu\text{m}$ electrode spacing.

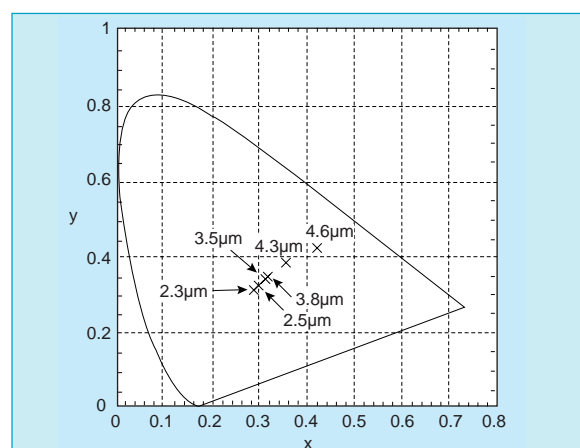


Fig. 5 Chromaticity (color coordinate) vs. panel gap at $10\mu\text{m}$ electrode spacing.

ing substrate, we found that static electricity accumulates at the outer edges of the panel, causing misalignment of the liquid crystals as though a field were applied along the screen's

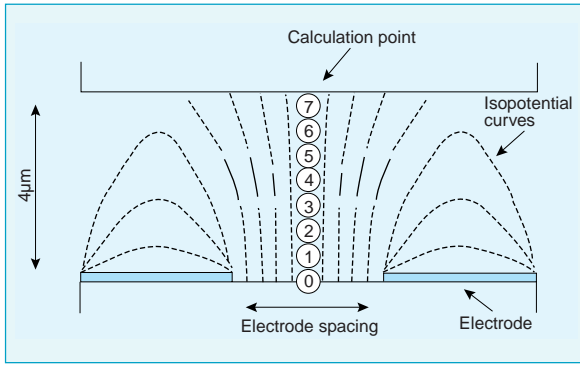


Fig. 6 Reference points for calculating the field between the interdigital electrodes.

vertical axis. We resolved this problem by applying a polarizing layer to the panel with conductive characteristics that prevent the generation of charge concentrations.

TFT Array Configuration

ELECTRODE SPACING. The spacing of the interdigital electrodes is a major determinant of pixel aperture ratio, but wider spacing requires a higher drive voltage, and the drive voltage is limited by the voltage rating of the thin-film transistor array and driver IC. The electrode spacing is set to use the highest available drive voltage.

FIELD SIMULATION. Spacing between the interdigital electrodes cannot be optimized by conventional simulation software because the field between the interdigital electrodes of IPS-mode displays is not uniform like the field between the panels of TN-mode displays. We therefore developed an original quasi-pragmatic simulation and used it to optimize interdigital electrode spacing.

As shown in Fig. 6, we established eight coordinate points at 0.5 μm intervals across the center of the electrode. We then calculated the electric field strength for various applied voltages and interdigital electrode spacings. These calculations assumed a 300nm silicon nitride protective film over the electrodes.

Fig. 7 shows the electric field intensity for electrode spacings of 8, 9 and 10 μm at applied voltages of 5 and 6V. For comparison, the figure also shows the field strength in an operational prototype display with a 10 μm electrode spacing and a 5.5V drive voltage.

We set a criterion for suitable designs as having a field intensity at all eight reference points higher than that of the prototype panel. At 8 μm spacing and a 5V drive voltage, the field intensity distribution nearly matched the standard, with room for a further rise in drive voltage. At a spacing of 9 μm, drive voltages in the 5~6V range are workable. At 10 μm spacing, a 6V drive

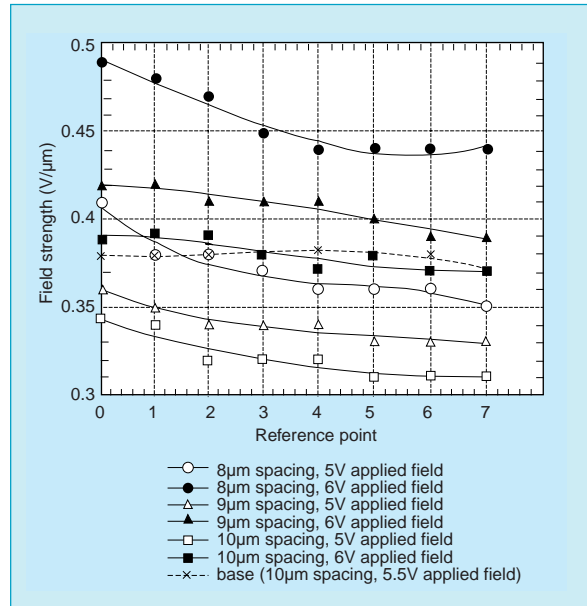


Fig. 7 Electric field strength.

voltage is necessary. Our driver ICs had a voltage rating of 5.5V, so we chose an electrode spacing of 9 μm.

PATTERN ACCURACY EFFECTS. Variations in the spacing between the interdigital electrodes cause field strength variations. These cause variations in pixel transmissivity that are visible as brighter or darker patches. Fig. 8 shows the results of a simulation of the effect of electrode width variations on display transmissivity. The variations are given as percentages relative to 50% transmissivity, midway between fully on and fully off states. Plots for three electrode widths are shown. These show that small variations in the electrode widths have a disproportionately large effect on brightness.

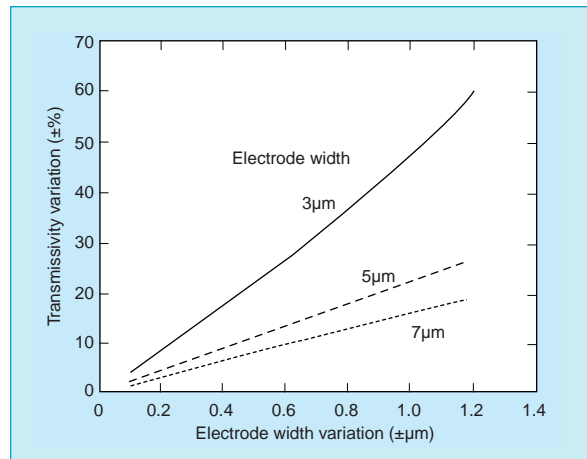


Fig. 8 Transmissivity variation vs. electrode width variation with 9 μm electrode spacing and 50% relative transmissivity.

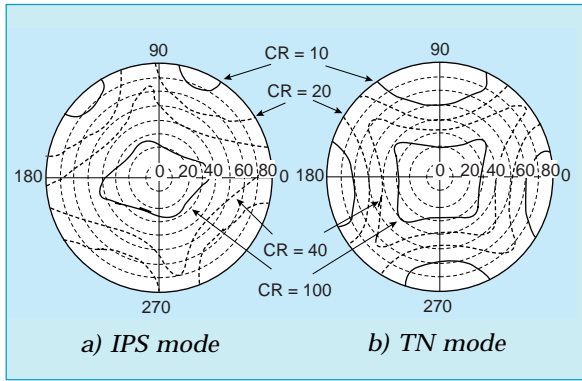


Fig. 9 Effect of viewing angle on contrast ratio for IPS and TN-mode displays.

We took two steps that have reduced these variations. We fabricated the electrodes from a thin (100nm) chrome film with a short etching time and produced the interdigital electrode in one process, improving registration accuracy. As a result, we were able to increase pattern accuracy for the interdigital electrodes to within $\pm 0.2\mu\text{m}$.

Optical Characteristics

Fig. 9 compares the viewing angle dependence of a prototype 15.1" IPS-mode XGA display incorporating the above findings with a TN-mode display using a retardation film to widen the viewing angle.

The iso-contrast contours in Fig. 9 increase from a low contrast ratio of 10 at the periphery toward a maximum contrast ratio of 100 at the center. The wider rings show that the new 15.1" XGA display has better wide-angle visibility than a TN-mode display, maintaining a con-

Table 1 Specifications of a Computer Display Monitor Using the Wide Viewing-Angle LCD Panel

Screen size	307.2 x 230.4mm (15.1" diagonal)
No. of pixels	1,024 x 768 (XGA)
Pixel aperture ratio	36%
Panel gap	3.5 μm
Electrode spacing	9 μm
Contrast ratio	150
Brightness	140cd/m ²
Viewing angle	Wider than 80° with contrast >10
Color inversion	Absent
Response time	60ms (sum of delays accompanying rise and decay)
White balance	(x, y) = (0.32, 0.34)

trast ratio of 10 or more at angles up to 80°.

Fig. 10 shows a direct view of the display image surrounded by 60°-views. Even at wide viewing angles, the display shows excellent contrast without color inversions. The display technology achieves wide-angle viewing with speed and white balance comparable to TN-mode displays. Table 1 lists major specifications.

This wide viewing-angle LCD monitor uses the IPS mode to permit viewing at angles wider than 80° with a contrast ratio of 10 or more. The display also retains the excellent response speed and color reproduction of TN designs, with adequate performance for PC monitor applications. The authors wish to acknowledge the cooperation of colleagues at Advanced Display Inc. □

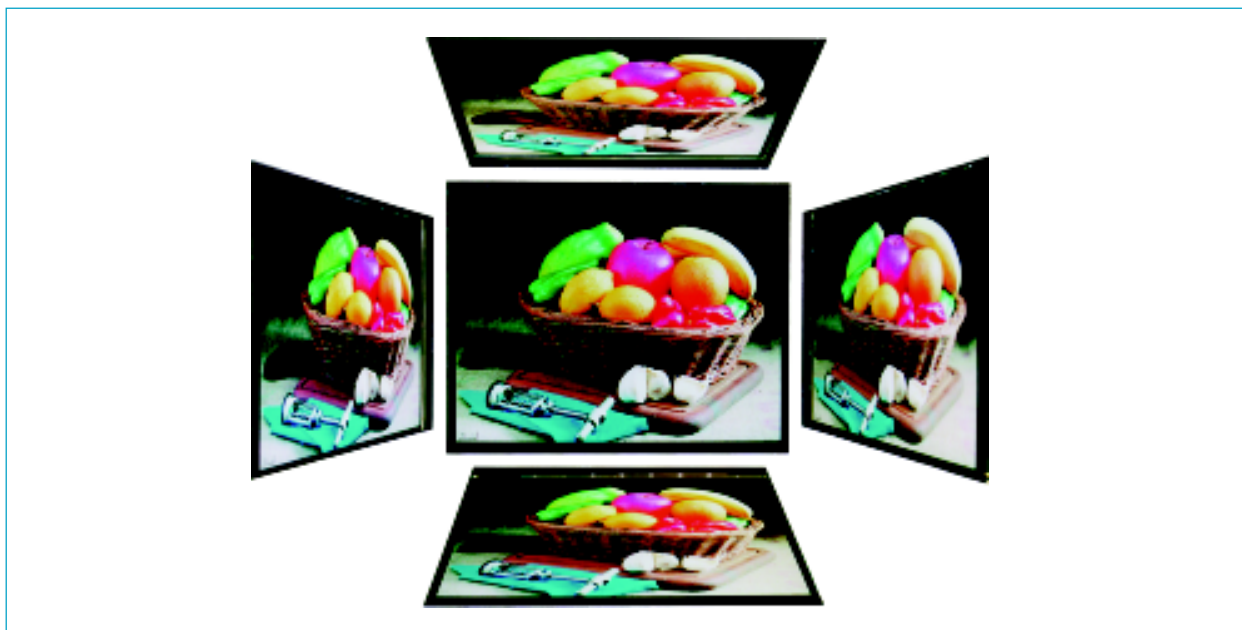


Fig. 10 Photographs of a prototype wide viewing-angle XGA monitor from different directions.

A 15.1-Inch XGA LCD Monitor

by Kazuyuki Iimura and Kunihiko Hashimoto*

Liquid-crystal display (LCD) monitors are a promising next-generation alternative to the CRT-based monitors used with most desktop computers. Mitsubishi Electric has recently developed its first stand-alone LCD monitor, a 15.1" active-matrix type with 1,024 × 768 (XGA) resolution. The LCD panel for the monitor was manufactured by Advanced Display Inc., a joint subsidiary of Asahi Glass Company and Mitsubishi Electric.

Features

The monitor's 15.1" (38cm) diagonal width provides a viewing area comparable to a 17" CRT monitor. Table 1 lists the main specifications.

Analog input with automatic frequency scanning provides compatibility with most current personal computers. The autotracking function handles horizontal frequencies from 31.5~60.2kHz and vertical frequencies from 56.3~85.1Hz.

The monitor houses an alternating current power supply in its base, complete with an adapter designed for worldwide use. The power supply carries three downstream universal serial bus (USB) hubs for connecting USB-compatible keyboards, mice, video cameras and other devices.

To facilitate maintenance, the monitor stores cumulative screen operating time, backlight operating time, and peak operating temperature. These values can be checked using the on-screen display and are stored in extended display identification (EDID) memory fields, permitting access from personal computers via the display data channel (DDC).

The cover protecting the LCD is a lightweight, cost-effective acrylic with an antireflection coating that improves contrast.

The monitor satisfies worldwide safety standards for electromagnetic interference, power factor correction, energy efficiency and ergonomics, including the strict regulations adopted by Sweden. The monitor's on-screen display is switchable among five languages: English, Dutch, French, German and Spanish.

Table 1 Specifications of Model LXA510PW LCD Monitor

LCD panel	
Type	Active matrix color LCD using thin-film transistors
Screen size (W × H)	307.2 × 230.4mm, 15.1-inch diagonal
Resolution (H × V)	1,024 × 768 pixels
Pixel dimensions (H × V)	0.3 × 0.3mm
Displayable colors	260,000
Brightness	200cd/m ²
Scanning frequencies	
Horizontal	31.5~60.2kHz
Vertical	59~85Hz
Input signals	
Type	Analog RGB, 0.7V _{pp}
Sync signal	Separate sync signal or TTL (positive or negative polarity)
Video signal impedance	75Ω
Sync signal impedance	1KΩ
User controls	
Front panel	Power switch
On-screen display	Brightness, contrast, screen position, color selection, color adjustment, clock frequency, clock phase, language, on-screen display duration, full-screen switching, power-saver mode, mode display, serial number display, reset
Connectors	Mini D-SUB15P for video input, two-conductor grounded AC cord
Ambient conditions	5~35°C, 20~80% humidity (no dew)
Power supply	90~264VAC, 50/60Hz
Power consumption	45W (55W with USB ports in use)
Tilt stand	Adjustable between -5° and +35°
Dimensions (H × D × W)	437 x 232.5 x 385mm
Weight	8.5kg
Preset operating modes	12 factory modes, 6 user modes

System Circuitry

Fig. 1 shows a block diagram of the monitor's circuitry. The analog RGB inputs are amplified and sent through an analog-to-digital converter (ADC) to a digital signal processor (DSP) that generates digital RGB signals for controlling the

*Kazuyuki Iimura and Kunihiko Hashimoto are with the Image & Information Systems Works.

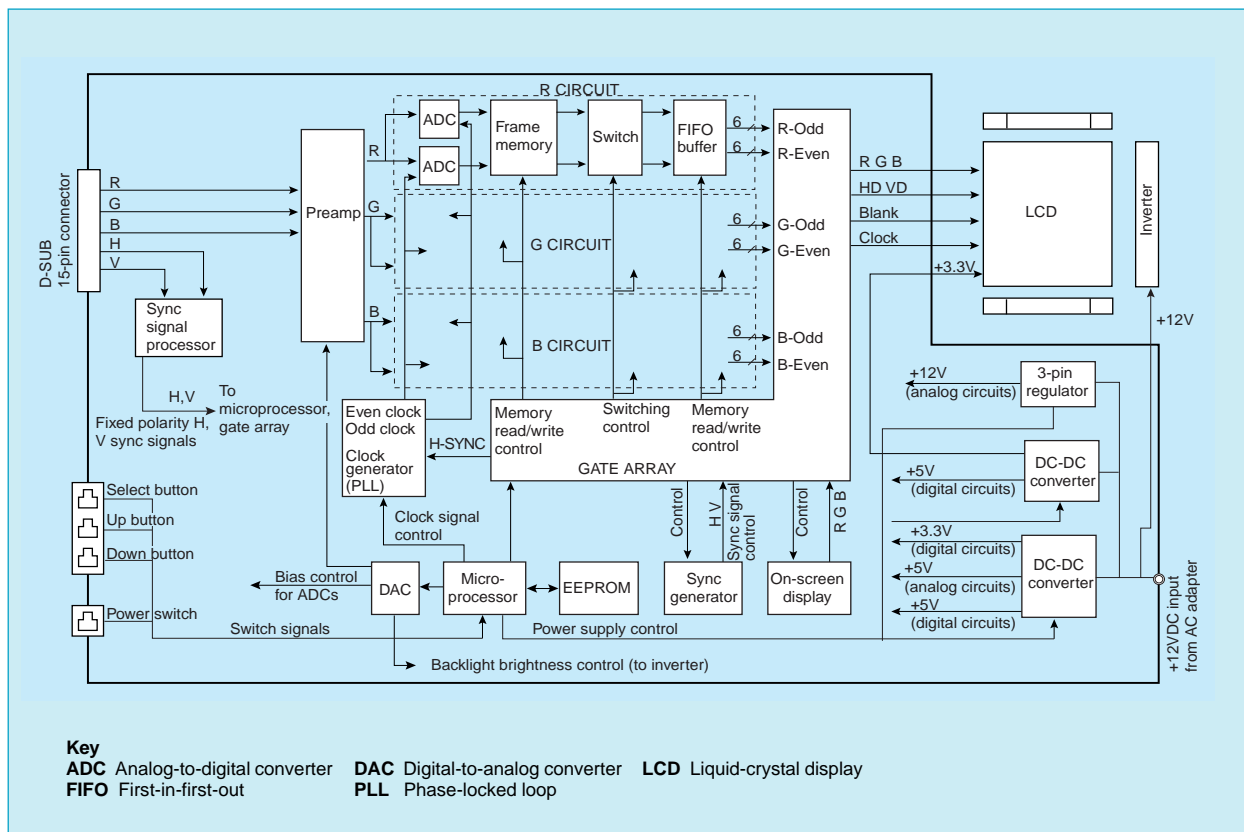


Fig. 1 A block diagram of the LCD monitor's main circuits.

LCD panel. A second power supply converts a single +12V supply to the various voltages needed to run the LCD panel and the inverter driving the display's two backlights. These circuits are controlled by a 16-bit microprocessor and a gate array.

SYNC SIGNAL PROCESSOR. This processor determines the polarity of the horizontal and vertical sync signals, generates a fixed-polarity synchronized clock signal and provides data for use by the microprocessor in selecting circuit control parameters from EEPROM tables.

PLL CONTROLLER. The ADC digitizes the analog input in step with a trigger signal. The trigger signal must be synchronized to the personal computer's horizontal dot clock or screen noise will appear. While a phase-locked loop (PLL)

reliably determines the correct frequency, manual adjustment available via the on-screen display enables the user to compensate for the phase differences occasionally seen among computer video adapters.

MEMORY CONTROLLER. The memory used in the process of digitizing the analog video input is controlled by the microprocessor and gate array. The microprocessor detects image resolution, extracts the appropriate memory control parameters from an EEPROM table, and passes these to the gate array which generates pulses controlling memory read and write operations (Fig. 2).

AUTOMATIC MODE CONTROL. Optimum parameters for 12 commonly used graphic modes are stored in EEPROM. In addition, the monitor

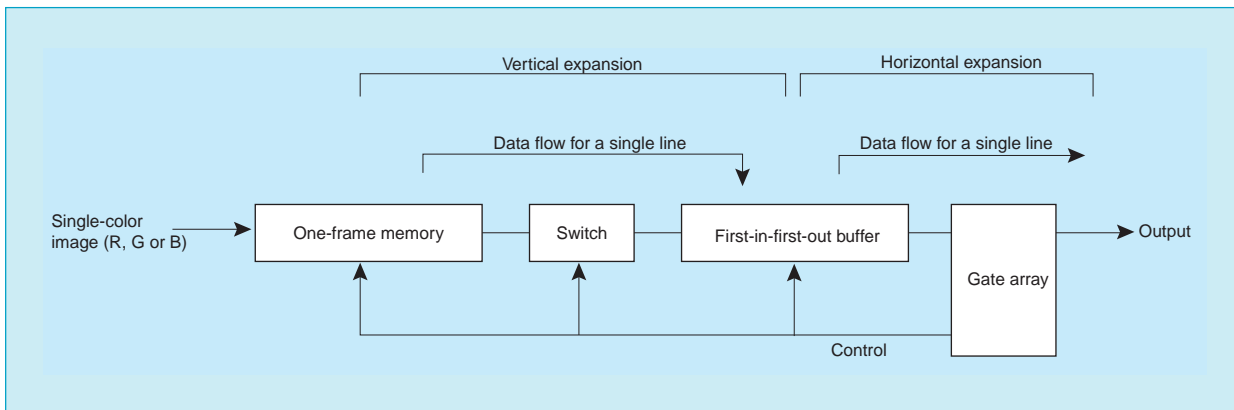


Fig. 2 Data flow for frame expansion function.

can store up to six sets of user-defined parameters for non-standard graphic modes. The system automatically computes appropriate characteristics for user-specified modes based on the horizontal scanning frequency and vertical refresh frequencies.

USB Circuits. The USB, a new serial interface for computer peripherals, has been designed with the support of numerous computer-related enterprises and has begun appearing in new-model personal computers. Each USB port has a bandwidth of 12Mbps, and connects to a high-speed (12Mbps) or low-speed (1.5Mbps) device. Each port can also supply up to 5V/500mA of power to peripherals, eliminating the need for separate AC adapters.

External Design

Engineered to maximize the space savings of the LCD-based design, the new monitor provides the viewing area of a 17" CRT monitor in a compact package, making it ideally suited to crowded offices where desk space is at a premium. Display dimensions are 437 x 232.5 x 385mm (H x D xW), giving it a footprint 60% smaller than our 17-inch CRT monitors, while the 8.5kg weight is less than half that of a CRT monitor. The tilt-stand is placed toward the rear of the monitor to leave room in front for a keyboard. The tilt-stand and power supply can also

be removed to allow mounting on a wall or swing-arm.

While CRT-style analog inputs and signal timing are being used at present, LCD panels can be improved by resolving the constraints of CRT displays such as the blanking period at the end of the frame. By developing a new video signal standard especially for LCD panels, a monitor could display video signals continuously, allowing the frequency of the horizontal dot clock to be reduced by 20%, which would lower the expense of the ADC and other components. □

Note: XGA is a registered trademark of IBM.

A TFT-LCD Panel for Thin Notebook Personal Computers

by Katsuhiko Honda and Mitsumasa Umesaki*

Mitsubishi Electric has developed the world's thinnest notebook-size personal computer using a 12.1-inch ultrathin active-matrix LCD panel. Although half the thickness of the panels in previous Mitsubishi notebook computers, this thoroughly redesigned product offers SVGA resolution (800 × 600 dots) with 37,728 displayable colors. Designed specifically to help achieve the ideal mobile office, the display incorporated is bright and power efficient.

Description

Fig. 1 shows a photo of the notebook computer and LCD panel. The complete computer is just 18mm thick, consisting of an 11.2mm bottom shell housing the computer and keyboard, and a 6.15mm hinged top shell with mounted LCD panel. The display is less than half the thickness of our previous comparable product. Table 1 lists the panel specifications.

Ribbed magnesium-alloy shells with an average thickness of just 1mm provide a rugged housing for the computer and display. Thixotropy



Fig. 1 This sleek notebook computer houses an LCD module just 6mm thick.

pic semi-solid molding, a type of injection molding, is used to fabricate the case, resulting in fewer sink marks and cracks than diecast construction. CAE-based mold-flow analysis and 3D structural analysis were used to ensure design integrity.

Display Construction

In order to save space, and in an innovative departure from previous practice, all display components are assembled directly into the display housing: the panel, interface circuit, driver LSI, and backlight power supply. Precision ribs on the housing hold the LCD panel and light guide. This design also reduces the component count and simplifies assembly.

The backlight for the display is a single 2mm-diameter cold-cathode fluorescent tube. The light guide is

2mm at its thickest point. Highly accurate ray-trace simulations were run to optimize the backlight reflector in a thin design with a small offset between the light guide and lamp.

A new gluing technique was developed to prevent wrinkles from developing due to different rates of thermal expansion in the layers of the panel optical system. It involves the use of a protection film, two lens films and diffusion film.

The thickness of the inverter circuit driving the backlight has been halved by using compact piezoelectric transformers, custom-manufactured low-profile connectors, and other specially designed components.

The LCD uses 0.7mm-thick glass for both the TFT substrate and the color filter. The design also eliminates a 0.5mm gap that was present

Table 1 Specifications of the LCD Panel

Module outline (W x H x D)	297 x 218 x 6.15mm
Weight	620g
Effective display area	246 x 184.5mm, 12.1" diagonal
Dot configuration	800 x 600
Dot pitch	0.125mm horizontal, 0.375mm vertical
Pixel configuration	RBG stripe (divided horizontally)
Display mode	Normally white
Display colors	37,728
Brightness	70cd/m ²
Backlight	Single cold-cathode fluorescent tube, edge-mounted, with inverter drive

*Katsuhiko Honda is with Advanced Display Inc. and Mitsumasa Umesaki the Advanced Technology R&D Center.



Fig. 2 Assembly cell for thin LCD displays. The previous thickness of 20mm was reduced to 6.2mm.

between the LCD panel and light guide in previous LCDs. This results in a thinner panel that excludes dust from the display interior.

Display Assembly Process

We developed a state-of-the-art LCD assembly line consisting of multiple assembly cells. The cell's operator places the housing, backlight and LCD panel onto a stage, then the cell assembles the display precisely and automatically. The operator is left to insert screws in the hinge and top cover. The assembly time is short, and the use of separate assembly cells restricts contamination by foreign particles. Fig. 2 shows an assembly cell.

Mitsubishi Electric is working diligently in the field of mobile computing to maintain its status as a world leader in information-processing technologies. Introduced under the name "Pedion" at COMDEX '97 in November of last year, this new notebook computer was voted first place in the Best of Comdex awards in the mobile computing category, reflecting the company's unending commitment to pioneering advancements in technology. □

NEW PRODUCTS

Advanced Color Thin-Film Transistor LCDs

Liquid-crystal displays are used extensively in notebook computers and many other applications, and there is a huge latent demand for products offering improved brightness, higher resolutions and wider viewing angles while maintaining the low power consumption and slim, lightweight construction of previous LCDs. Mitsubishi Electric has developed four new LCDs that offer significant advances in this direction.

MODEL AA084VB01—8.4" (21cm) DIAGONAL. Use of a retardation film gives this LCD a wide viewing angle range of 120° horizontally and 90° vertically, with bright, 200cd/m² optical output. The product targets applications in measuring instruments and factory automation equipment.

MODEL AA121SG11—12.1" (31cm) DIAGONAL. Intended for notebook computer applications, this display features a thickness of 5.9mm (reduced from 8.0mm) and a weight of 395g (reduced from 500g.) Improvements in panel transmissivity and backlight efficiency have boosted panel brightness fully 50% to 150cd/m².

MODEL AA141XA01—14.1" (36cm) DIAGONAL. The largest LCD panel in the industry commercially available as we go to press, this product offers 1,024 x 768 resolution in a thin, lightweight and narrow-frame design fitted with an LVDS interface. It is intended for high-end notebook computer applications.

MODEL AA151XB11—15.1" (38cm) DIAGONAL. Still larger, this display aims to compete with CRTs for desktop monitoring applications. The display can be viewed over a range of 100° in both horizontal and vertical planes, while brightness has been increased to 200cd/m². □



MODEL AA084VB01



MODEL AA141XA01



MODEL AA121SG11



MODEL AA151XB11

*Portions of the displays are taken from the Kodak Photo CD Sampler with Film.

Specifications

Units	AA084VB01	AA121SG01	AA141XC01	AA151XB11
Panel size	8.4" (21.4cm)	12.1" (30.8cm)	14.2" (36.1cm)	15.1" (38.4cm)
Resolution (H x V)	640 x 480	800 x 600	1,024 x 768	1,024 x 768
Pixel pitch	0.267mm	0.3075mm	0.282mm	0.300mm
Displayable colors	262,000	262,000	262,000	262,000
Brightness	200cd/m ²	150cd/m ²	150cd/m ²	210cd/m ²
Backlight configuration	Replaceable CCFT* (2)	CCFT (1)	CCFT (1)	Replaceable CCFT (4)
Contrast ratio	150:1	150:1	150:1	150:1
Viewable angle (maintaining a contrast of at least 10:1)				
Horizontal	60°	45°	45°	60°
Vertical	-40°~ +50°	-30°~ +10°	-30°~ +10°	-60°~ +40°
Interface	CMOS	LVDS, 40MHz	LVDS, 65MHz	CMOS
Power supply	3.3V	3.3V	3.3V	3.3V, 12V
Power consumption	3.0W	3.9W	4.7W	24.5W
Dimensions (mm) (W x H x D)	221.0x152.4x10.6	275.0x199.0x5.9	298.5x227.0x7.5	355.2x269.8x23.0
Weight	420g	395g	610g	2.0kg

* Cold cathode fluorescent tube.

MITSUBISHI ELECTRIC OVERSEAS NETWORK (Abridged)

Country	Address	Telephone	
U.S.A.	Mitsubishi Electric America, Inc.	5665 Plaza Drive, P.O. Box 6007, Cypress, California 90630-0007	714-220-2500
	Mitsubishi Electronics America, Inc.	5665 Plaza Drive, P.O. Box 6007, Cypress, California 90630-0007	714-220-2500
	Mitsubishi Consumer Electronics America, Inc.	2001 E. Carnegie Avenue, Santa Ana, California 92705	714-261-3200
	Mitsubishi Semiconductor America, Inc.	Three Diamond Lane, Durham, North Carolina 27704	919-479-3333
	Horizon Research, Inc.	1432 Main Street, Waltham, Massachusetts 02154	617-466-8300
	Mitsubishi Electric Power Products Inc.	Thorn Hill Industrial Park, 512 Keystone Drive, Warrendale, Pennsylvania 15086	412-772-2555
	Mitsubishi Electric Manufacturing Cincinnati, Inc.	4773 Bethany Road, Mason, Ohio 45040	513-398-2220
	Astronet Corporation	37 Skyline Drive, Suite 4100, Lake Mary, Florida 32746-6214	407-333-4900
Canada	Powerex, Inc.	Hills Street, Youngwood, Pennsylvania 15697	412-925-7272
	Mitsubishi Electric Research Laboratories, Inc.	201 Broadway, Cambridge, Massachusetts 02139	617-621-7500
Mexico	Mitsubishi Electric Sales Canada Inc.	4299 14th Avenue, Markham, Ontario L3R 0J2	905-475-7728
	Mitsubishi Electronics Industries Canada Inc.	1000 Wye Valley Road, Midland, Ontario L4R 4L8	705-526-7871
Brazil	Melco de Mexico S.A. de C.V.	Mariano Escobedo No. 69, Tlalnepantla, Edo. de Mexico	5-565-6269
	MELCO do Brazil, Com. e Rep. Ltda.	Av. Rio Branco, 123, a 1507, 20040, Rio de Janeiro	21-221-8343
Argentina	MELCO-TEC Rep. Com. e Assessoria Tecnica Ltda.	Av. Rio Branco, 123, a 1507, 20040, Rio de Janeiro	21-221-8343
	MELCO Argentina S.R.L.	Florida 890-20º-Piso, C.P. 1005, Buenos Aires	1-312-6982
Colombia	MELCO de Colombia Ltda.	Calle 35 No. 7-25, Oficinas No. 1201/02, Edificio, Caxdac, Apartado Aereo 29653, Bogotá	1-287-9277
U.K.	Mitsubishi Electric U.K. Ltd.	Travellers Lane, Hatfield, Herts. AL10 8XB, England	1707-276100
	Apricot Computers Ltd.	3500 Parkside, Birmingham Business Park, Birmingham, B37 7YS, England	21-717-7171
	Mitsubishi Electric Europe Coordination Center	Centre Floor (18th Floor), 103 New Oxford Street, London, WC1A 1EB	71-379-7160
France	Mitsubishi Electric France S.A.	25 Boulevard des Bouvets, 92741 Nanterre Cedex	1-55-68-55-68
Netherlands	Mitsubishi Electric Netherlands B.V.	3rd Floor, Parnassustoren, Locatellikade 1, 1076 AZ, Amsterdam	20-6790094
Germany	Mitsubishi Electric Europe GmbH	Gothaer Strasse 8, 40880 Ratingen	2102-4860
	Mitsubishi Semiconductor Europe GmbH	Konrad Zuse Strasse 1, 52477 Alsdorf	2404-990
Spain	MELCO Iberica S.A. Barcelona Office	Poligono Industrial "Can Magi", Calle Joan Buscallà 2-4, Apartado de Correos 420, 08190 Sant Cugat del Vallés, Barcelona	3-589-3900
Italy	Mitsubishi Electric Europe GmbH, Milano Office	Centro Direzionale Colleoni, Palazzo Perseo-Ingresso 2, Via Paracelso 12, 20041 Agrate Brianza, Milano	39-60531
China	Shanghai Mitsubishi Elevator Co., Ltd.	811 Jiang Chuan Rd., Minhang, Shanghai	21-4303030
Hong Kong	Mitsubishi Electric (H.K.) Ltd.	41st Floor, Manulife Tower, 169 Electric Road, North Point	510-0555
	Ryoden Holdings Ltd.	10th Floor, Manulife Tower, 169 Electric Road, North Point	887-8870
	Ryoden Merchandising Co., Ltd.	32nd Floor, Manulife Tower, 169 Electric Road, North Point	510-0777
Korea	KEFICO Corporation	410, Dangjung-Dong, Kunpo, Kyunggi-Do	343-51-1403
Taiwan	MELCO Taiwan Co., Ltd.	2nd Floor, Chung-Ling Bldg., No. 363, Sec. 2, Fu-Hsing S. Road, Taipei	2-733-2383
	Shihlin Electric & Engineering Corp.	No. 75, Sec. 6, Chung Shan N. Rd., Taipei	2-834-2662
	China Ryoden Co., Ltd.	Chung-Ling Bldg., No. 363, Sec. 2, Fu-Hsing S. Road, Taipei	2-733-3424
Singapore	Mitsubishi Electric Singapore Pte. Ltd.	152 Beach Road #11-06/08, Gateway East, Singapore 189721	295-5055
	Mitsubishi Electric Sales Singapore Pte. Ltd.	307 Alexandra Road #05-01/02, Mitsubishi Electric Building, Singapore 159943	473-2308
	Mitsubishi Electronics Manufacturing Singapore Pte. Ltd.	3000, Marsiling Road, Singapore 739108	269-9711
	Mitsubishi Electric Asia Coordination Center	307 Alexandra Road #02-02, Mitsubishi Electric Building, Singapore 159943	479-9100
Malaysia	Mitsubishi Electric (Malaysia) Sdn. Bhd.	Plo 32, Kawasan Perindustrian Senai, 81400 Senai, Johor	7-5996060
	Antah MELCO Sales & Services Sdn. Bhd.	3 Jalan 13/1, 46860 Petaling Jaya, Selangor, P.O. Box 1036	3-756-8322
	Ryoden (Malaysia) Sdn. Bhd.	2nd Fl., Wisma Yan, Nos. 17 & 19, Jalan Selangor, 46050 Petaling Jaya	3-755-3277
Thailand	Kang Yong Watana Co., Ltd.	15th Floor, Vanit Bldg., 1126/1, New Petchburi Road, Phayathai, Bangkok 10400	2-255-8550
	Kang Yong Electric Co., Ltd.	67 Moo 11, Bangna-Trad Highway, Km. 20 Bang Plee, Samutprakarn 10540	2-312-8151
	MELCO Manufacturing (Thailand) Co., Ltd.	86 Moo 4, Km. 23 Bangna-Trad, Bangplee, Semudparkarn 10540	2-312-8350-3
	Mitsubishi Elevator Asia Co., Ltd.	Bangpakong Industrial Estate, 700/86-92, Moo 6 Tambon Don Hua Roh, Muang District Chonburi 20000	38-213-170
Philippines	Mitsubishi Electric Asia Coordination Center (Thailand)	17th Floor, Bangna Tower, 2/3 Moo 14, Bangna-Trad Highway 6.5 Km, Bangkawe, Bang Plee, Samutprakarn 10540	2-312-0155-7
	International Elevator & Equipment, Inc.	Km. 23 West Service Road, South Superhighway, Cupang, Muntinlupa, Metro Manila	2-842-3161-5
Australia	Mitsubishi Electric Australia Pty. Ltd.	348 Victoria Road, Postal Bag No. 2, Rydalmere, N.S.W. 2116	2-684-7200
New Zealand	MELCO Sales (N.Z.) Ltd.	1 Parliament St., Lower Hutt, P.O. Box 30-772 Wellington	4-569-7350
Representatives			
China	Mitsubishi Electric Corp. Beijing Office	SCITE Tower, Rm. 1609, Jianguo Menwai, Dajie 22, Beijing	1-512-3222
	Mitsubishi Electric Corp. Shanghai Office	Room No. 1506-8, Shanghai Union Building 100, Yanan-East Street, Shanghai	21-320-2010
Korea	Mitsubishi Electric Corp. Seoul Office	Daehan Kyoyuk Insurance Bldg., Room No. 1204 #1, Chongno 1-ka, Chongno-ku, Seoul	2-732-1531-2
Viet Nam	Mitsubishi Electric Corp. Ho Chi Minh City Office	8 B2, Han Nam Officetel 65, Nguyen Du St., 1st District, Ho Chi Minh City	8-243-984

